Acta Geotechnica (2022) 17:355–376
https://doi.org/10.1007/s11440-021-01155-3

RESEARCH PAPER

A novel approach of random packing generation of complex-shaped 3D particles with controllable sizes and shapes

Xiang Wang[1,3] · Zhen-Yu Yin[3] · Dong Su[1,2] · Xiaoxin Wu[4] · Jidong Zhao[5]

Received: 26 July 2020 / Accepted: 26 January 2021 / Published online: 29 May 2021

Abstract

This paper presents a novel computational-geometry-based approach to generating random packing of complex-shaped 3D particles with quantitatively controlled sizes and shapes for discrete modeling of granular materials. The proposed method consists of the following five essential steps: (1) partitioning of the packing domain into a prescribed number of random polyhedrons with desired sizes and form-scale shapes using the constrained Voronoi tessellation; (2) extraction of key points from the edges and facets of each polyhedron; (3) construction of a freeform curve network in each polyhedron based on Bézier curve fitting; (4) generation of solid particles with smooth, convex surfaces using the biharmonic-based surface interpolation of the constructed network; and (5) creation of concavity by superimposing spherical harmonic-based random noise. To ensure that the obtained shape descriptors (e.g., the elongation, flatness, roundness and convexity ratio) match the hypothesized values, an inverse Monte Carlo algorithm is employed to iteratively fine-tune the control parameters during particle generation. The ability of the proposed approach to generate granular particles with the desired geometric properties and packing is demonstrated through several examples. This study paves a viable pathway for realistic modeling of granular media pertaining to various engineering and industrial processes.

Keywords Bézier curve fitting · Biharmonic equation · Complex-shaped particles · Granular packing · Spherical harmonics · Surface interpolation · Voronoi tessellation

✉ Dong Su
sudong@szu.edu.cn

Xiang Wang
xiang.wang@polyu.edu.hk

Zhen-Yu Yin
zhenyu.yin@polyu.edu.hk

Xiaoxin Wu
1301150334@csu.edu.cn

Jidong Zhao
jzhao@ust.hk

[1] College of Civil and Transportation Engineering, Shenzhen University, Shenzhen, China

[2] Key Laboratory of Coastal Urban Resilient Infrastructures (MOE), Shenzhen University, Shenzhen, China

[3] Department of Civil and Environmental Engineering, The Hong Kong Polytechnic University, Hung Hom, Kowloon, Hong Kong, China

[4] Department of Mathematics and Statistics, Central South University, Changsha, Hunan, China

[5] Department of Civil and Environmental Engineering, Hong Kong University of Science and Technology, Hong Kong, China

1 Introduction

The geometric and morphological properties of particles, including the size, form, corner sharpness, concavity and surface roughness, play distinct important roles in affecting the macro- and micromechanical behaviors of granular materials. This has been evidenced by numerous laboratory experiments [1, 2, 14, 36, 41, 46, 48] and numerical simulations [8, 40, 43, 50]. Microscopically, the various geometric features of a particle may affect its interactions and motions with the surrounding particles in a granular assembly, which collectively dictates the overall mechanical responses of the material. For example, the form (elongation and flatness) and the corner sharpness (roundness) tend to affect the rolling motion of a particle, while the concavity (convexity ratio) may cause interlocking at the contacts between particles. To differentiate the unique effect of each individual geometric feature towards understanding of their collective influence on the overall behavior of a granular assembly, numerical generation of

discrete particles with independent size or shape characteristics of interest appears to be a viable (if not the only) option.

Indeed, discrete modeling of granular media has received increasing popularity across many scientific and engineering fields, including chemical engineering [7, 10, 55], powder engineering [20, 23, 42] and civil/geotechnical engineering [9, 17, 37]. In particular, the discrete element method (DEM) prevails among many discrete modeling approaches for investigating the microscopic and macroscopic behaviors of granular materials [31, 35, 44]. Within the general framework of the DEM, a variety of approaches have been developed to generate particles with different geometries for DEM simulations. Taking the form as an example, Ng [29] developed a DEM using elliptical particles to study the mechanical behavior of idealized granular materials under 2D conditions, which was further extended to 3D ellipsoid particles [15, 24, 25]. Other relevant studies include the use of elongated particles with rounded caps to examine the effects of elongation [4] and spherocylindrical particles to study the effects of different aspect ratios [22, 32] on granular behavior. Other studies have focused on shape features other than the form. For example, superellipsoid particles [51] and superquadric particles [19] have been used to simulate ellipsoid-like particles with different degrees of angular sharpness at the corners in discrete element simulations. Particles with asymmetric shapes but smooth surfaces have also been proposed, such as egg-shaped particles [53] and polyellipsoid particles [33]. Random simple convex polyhedral particles [28] have also been proposed to simulate real particle shapes, but with rather limited quantitative control of the shape features. Other recent efforts have focused on employing spectrum-based methods, including the Fourier series [27] and spherical harmonics [38, 52], to generate realistic particles with complex shapes. The generated shape features are statistically correlated with the adopted Fourier series or spherical harmonics coefficients. However, these spectrum-based approaches are not without limitations. For example, they cannot adequately and independently control the corner sharpness and the concavity features. As stated in [27], real sand grains exhibit some planar facets and sharp corners. These features are not reproduced well by spectrum-based methods, which usually disregard the potential correlation between the phase angles of each harmonic in the frequency domain and assume that the phase angles are statistically independent random variables.

This study presents the development of a more robust technique for grain shape reconstruction. In particular, it is aimed to generate random packing of irregular-shape particles with quantitative, independent control of key geometrical features, including the particle size (average radius), form (elongation and flatness), corner sharpness (roundness), and concavity (convexity ratio). The proposed algorithms are developed based on three areas of previous work by the authors: (1) the Fourier–Voronoi-based packing of star-like particles [27]; (2) the spherical-harmonics-based generation of realistic sand particles [39, 52]; and (3) dense packing of convex granules based on Voronoi tessellation and cubic-polynomial-curve fitting [47]. First, the constrained Voronoi tessellation is employed to partition a sample domain into irregular polyhedrons, namely the Voronoi cells. The obtained polyhedrons are employed as the basic elements for the particle generation. The curve fitting technique is then extended to generate 3D convex particles that are inscribed to the Voronoi cell, and the edge midpoints and facet centers are extracted from each polyhedron as the key points of the particle outline. The Bézier curve fitting is employed to construct a curve network that passes through the extracted key points. Next, the biharmonic equation is employed to develop a unique surface interpolation algorithm to generate a solid particle with a closed smooth surface that is bounded by the Bézier curve network. Finally, based on the inverse operation of spherical harmonics transformation, the particle concavity features are quantitatively reproduced by superimposing the amplitude-controlled harmonic series of certain frequencies. To make the generated non-spherical shapes resemble the desired targets, the inverse Monte Carlo approach is employed to adjust the sizes and shapes of the generated particles, so that the obtained geometry statistically approximates the desired one. To further demonstrate the capability of the proposed algorithms, three scenarios of granular particles packing are generated with distinctive sizes and shapes that approximate the prescribed targets. The proposed work paves a pathway to further DEM-based studies of individual particle shape effects of each geometrical features (e.g., form, corner sharpness, concavity) on the macro- and micromechanical properties of granular materials.

2 Random generation of irregular particles

Random polyhedrons with irregular shapes have been performed in previous studies for simulations of granular particles [6, 11, 34]. However, the generated polyhedrons frequently exhibit unrealistic sharp corners and idealized convex surface, which fail to capture the geometric features of realistic granular particles, e.g., the corner sharpness and surface concavity. In this section, we first generate an assembly of random polyhedrons using Voronoi tessellation. Then, inside polyhedrons, we generate random complex-shaped particles with quantitatively controlled

geometric features based on a series of computational geometry algorithms and spherical harmonics.

2.1 Polyhedron generation and key point extraction

The Voronoi tessellation has been widely used in computational geometry [13]. It is employed here to randomly generate irregular polyhedrons. Typically, a random cloud of seeding points are first generated in a given domain which is then partitioned into a number of polyhedrons accordingly. The procedure is demonstrated in Fig. 1. First, as shown in Fig. 1a, a cubic box with unit side length is generated as the sample domain. Then, as shown in Fig. 1b, 20 points are randomly distributed inside a cubic domain. Next, Delaunay triangulation is performed to identify neighboring points, as shown in Fig. 1c. Finally, for each point, the corresponding polyhedron (Voronoi cell) is generated, as illustrated in Fig. 1d. In this study, each polyhedron is isolated as an individual container. Each container will be filled with a particle and the particle will be encompassed by the facets of the polyhedron. The overall shape of the particle is expected to approximate the given polyhedron to a certain extent.

For each polyhedron, a series of key points are extracted from its facets and edges. An example polyhedron is selected from the generated polyhedron for particle generation, as demonstrated in Fig. 2a. It is shown in Fig. 2b that both the midpoint (in cyan) of each side edge (in black solid line) and the center point (in red) of each polyhedron facet are extracted as the key points. As illustrated in Fig. 2c, since each edge of the polyhedron is naturally shared by two neighboring facets, each edge midpoint M_{edge} can be connected with two facet center points C^{l}_{facet} and C^{R}_{facet} (connected by a blue dashed line). In the next section, each group of key points (one edge midpoint and the neighboring facet midpoints, as highlighted in Fig. 2d) will be used to generate the curve network.

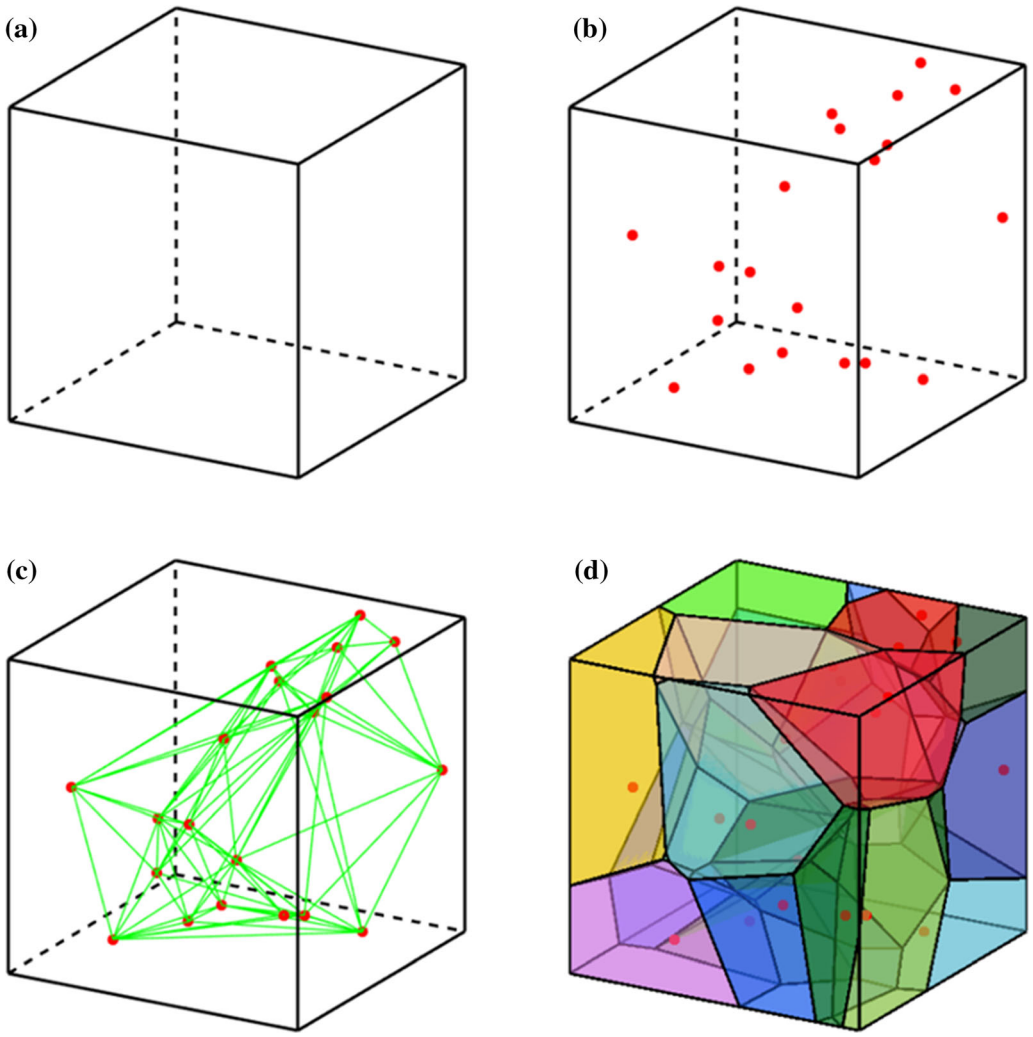

Fig. 1 Generation of irregular polyhedrons **a** define the sample domain; **b** node generation; **c** Delaunay triangulation; **d** Voronoi tessellation

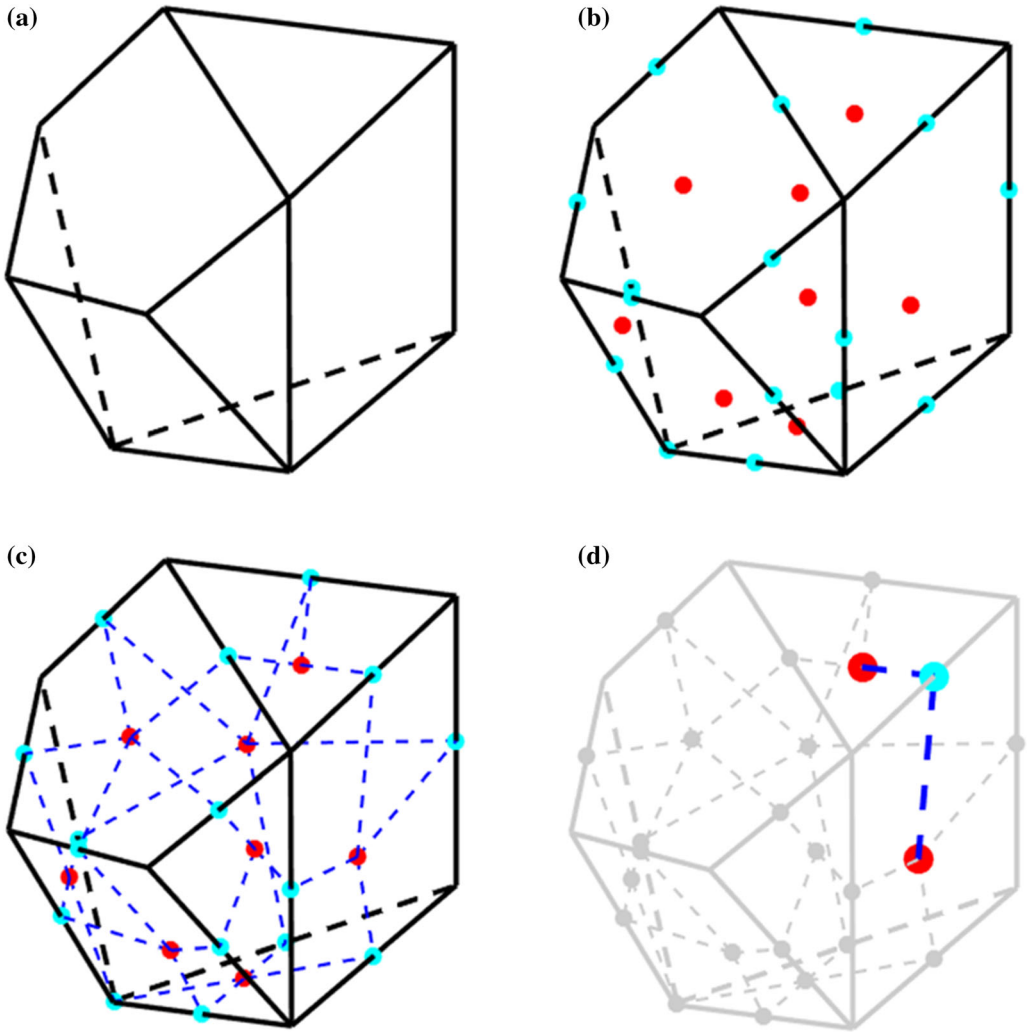

Fig. 2 Extraction of control points from the simple polyhedron

2.2 Generation of freeform curve network from key points

For an example corner $\angle C^l_{\text{facet}} M_{\text{edge}} C^R_{\text{facet}}$ (shown in Fig. 3a), which is formed by connecting an edge center point M_{edge} with two neighboring facet center points C^l_{facet} and C^R_{facet}, two additional control points Q_1 and Q_2 (highlighted as green points in Fig. 3b) are defined based on a curve fitting parameter w, where, $\text{w} \in [0, 1]$.

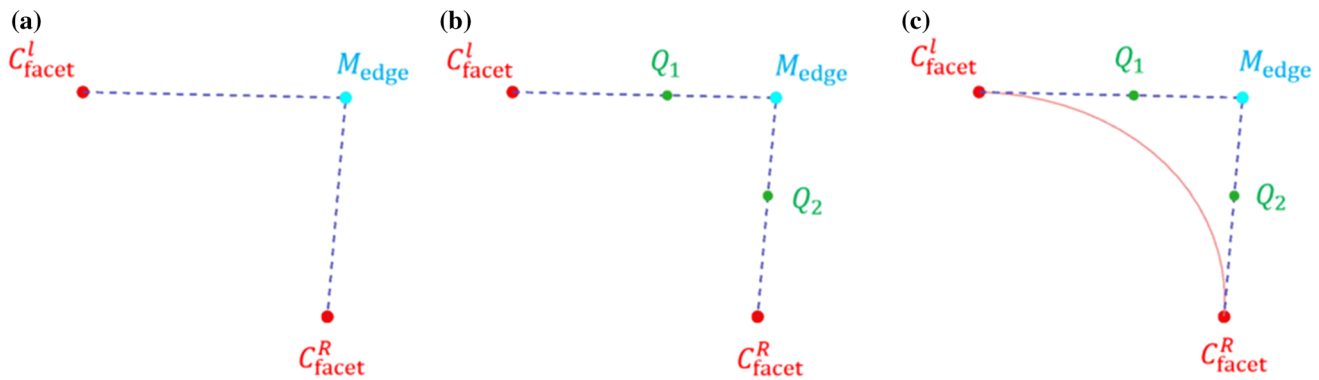

Fig. 3 Fitting the Bezier curve based on the extracted controlled points

$$Q_1 = (1-w)C^l_{\text{facet}} + wM_{\text{edge}} \tag{1}$$

$$Q_2 = (1-w)C^R_{\text{facet}} + wM_{\text{edge}} \tag{2}$$

$C^l_{\text{facet}}, C^R_{\text{facet}}, Q_1$ and Q_2 are thereby regarded as four control points to generate a cubic Bezier curve, which is tangentially oriented to lines $C^l_{\text{facet}}M_{\text{edge}}$ and $C^R_{\text{facet}}M_{\text{edge}}$ at C^l_{facet} and C^R_{facet}, respectively. The generated cubic Bezier curve (shown as a red solid curve in Fig. 3c) is expressed as follows:

$$B(u) = \sum_{i=0}^{3} B_i^3(u)P_i \tag{3}$$

where P_0 is set as C^l_{facet}, P_1 is set as Q_1, P_2 is set as Q_2, and P_3 is set as C^R_{facet}; the parametric domain of $B(u)$ is given by $u \in [0,1]$. $B_i^3(u)$ is the following cubic basis function

$$B_i^3(u) = \frac{3!}{i!(3-i)!}u^i(1-u)^{3-i} \tag{4}$$

The generated Bezier curves with three different shape parameter values ($w = 0.4, 0.6$ and 0.8) are illustrated in Fig. 4. When w increases, Q_1 and Q_2 become closer to M_{edge} but farther from C^l_{facet} and C^R_{facet}, and the generated curve more closely reflect the triangular corner $\angle C^l_{\text{facet}}M_{\text{edge}}C^R_{\text{facet}}$.

The above Bezier curve generation process is repeated for each triangular corner of the extracted key points, and finally, a freeform curve network is constructed from the simple target polyhedrons, as shown in Fig. 5.

2.3 Creating the particle surface from the curve network

Because the terminal vertex of each curve overlaps with the facet center point of the polyhedron, the generated curve network has a dual topology relation with the provided polyhedron. That is, each vertex v_i (in dark blue) of the given polyhedron corresponds to a curve area CF_i, which is bounded by three or four curves in the curve network. As shown in Fig. 6, one curve area CF_i in the curve network is bounded by 3 curves, B_0, B_1 and B_2, which are generated from three triangular corners $\angle C^l_{\text{facet}}M_{\text{edge}}C^R_{\text{facet}}$, and the edges and facets share the same vertex v_i. Based on this relation, the biharmonic equation is employed to generate a curved surface for the curve area in the generated curve network.

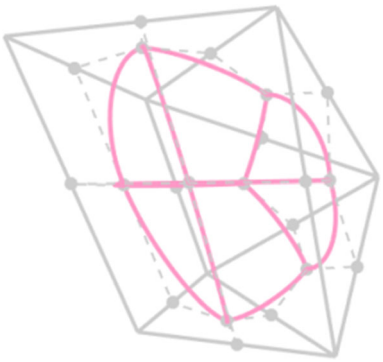

Fig. 5 Illustration of the generated freeform curve network

In this paper, we apply the biharmonic equations for smooth surface generation, which mainly focus on the generation of N-sided surface patch using biharmonic equation in the polar coordinates. The biharmonic equation falls into the category of elliptic partial differential equations (PDEs) and is commonly denoted by:

$$\Delta^2 \boldsymbol{u} = 0 \tag{5}$$

where Δ^2 represents the Laplace operator and u represents either of the x, y, z dimensions. The form of the Laplace operator in polar coordinates is:

$$\Delta^2 = \left[\frac{\partial^2}{\partial r^2} + \frac{1}{r}\frac{\partial}{\partial r} + \frac{1}{r^2}\frac{\partial^2}{\partial \theta^2}\right]^2 \tag{6}$$

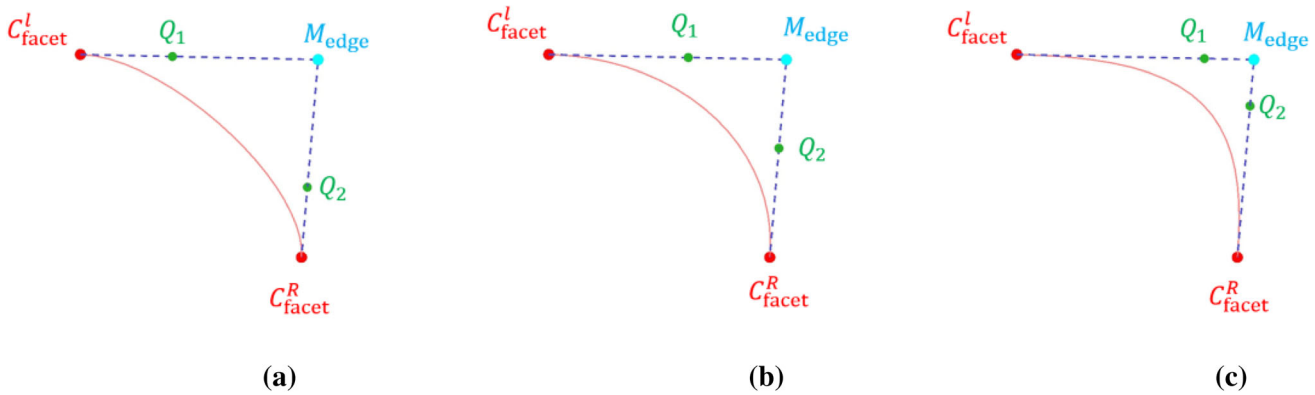

Fig. 4 Fitting the Bezier curve based on the extracted controlled points when **a** w=0.4; **b** w=0.6; and **c** w=0.8

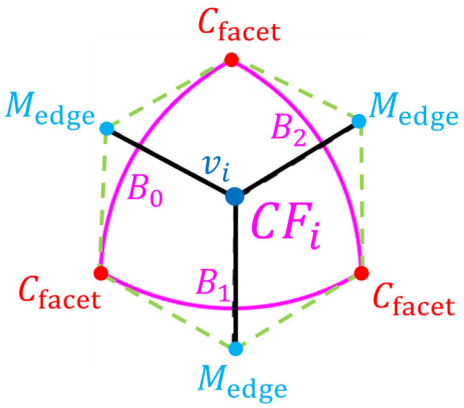

Fig. 6 Curve area CF_i corresponding to vertex v_i of the given polyhedron

In this section, Eq. (6) is employed as a mapping from [0,2π]×[0,1] to the curve area bounded by the N-sided Bezier curves. In order to solve Eq. (6), the boundary conditions are given by:

$$u(1,\theta) = f(\theta), \quad 0 \le \theta \le 1 \tag{7}$$

$$\left.\frac{\partial u}{\partial r}\right|_{r=1} = g(\theta), \quad 0 \le \theta \le 2\pi \tag{8}$$

where $f(\theta)$ s in x, y, z dimensions describe the N-sided boundary conditions and $g(\theta)$ s in x, y, z dimensions control the tendency of surface generation at r direction on the boundaries, which decide the normal direction n of generated surface on the boundaries by:

$$n = \left(\frac{\partial f}{\partial \theta} \times g(\theta)\right) / \left(\left|\frac{\partial f}{\partial \theta}\right| \cdot |g(\theta)|\right) \tag{9}$$

which can be modified through adjusting $g(\theta)$ s on three dimensions to make the adjacent surfaces satisfy a high continuity.

More specifically, the solution of (5) together with boundary conditions (7) and (8) can be obtained easily and efficiently in the form as follows:

$$u(r,\theta) = \frac{a_0}{2} + \frac{b_0}{4} r^2 + \sum_{n=1}^{\infty} r^n \left[\left(a_n + c_n r^2\right) cos\, n\theta + \left(b_n + d_n r^2\right) sin\, n\theta\right] \tag{10}$$

when $f(\theta)$ and $g(\theta)$ can be expressed in the Fourier series:

$$u(1,\theta) = f(\theta), \quad 0 \le \theta \le 1 \tag{11}$$

$$\left.\frac{\partial u}{\partial r}\right|_{r=1} = g(\theta), \quad 0 \le \theta \le 2\boldsymbol{\pi} \tag{12}$$

where α, β, δ and η can be obtained by fast Fourier transform:

$$a_n = \frac{1}{\pi}\int_0^{2\pi} f(\theta) cos\,(n\theta) d\theta \tag{13}$$

$$\beta_n = \frac{1}{\pi}\int_0^{2\pi} f(\theta) sin\,(n\theta) d\theta \tag{14}$$

$$\delta_n = \frac{1}{\pi}\int_0^{2\pi} g(\theta) cos\,(n\theta) d\theta \tag{15}$$

$$\eta_n = \frac{1}{\pi}\int_0^{2\pi} g(\theta) sin\,(n\theta) d\theta \tag{16}$$

or the discrete Fourier transform when the boundary conditions are given discretely as $f(\theta_i)$ and $g(\theta_i)$, i= 1, 2, 3, …, N (θ_N=2π) with the intervals denoted as s_i:

$$a_n = \frac{1}{\pi} mean[f(\theta_i)\cos(\mathrm{n}\theta_\mathrm{i})\theta_\mathrm{i}] \tag{17}$$

$$\beta_n = \frac{1}{\pi} mean[f(\theta_i)\sin(\mathrm{n}\theta_\mathrm{i})\theta_\mathrm{i}] \tag{18}$$

$$\delta_n = \frac{1}{\pi} mean[g(\theta_i)\cos(\mathrm{n}\theta_\mathrm{i})\theta_\mathrm{i}] \tag{19}$$

$$\eta_n = \frac{1}{\pi} mean[g(\theta_i)\sin(\mathrm{n}\theta_\mathrm{i})\theta_\mathrm{i}] \tag{20}$$

Additionally, the coefficients in Eq. (10) can be obtained through variable separation as follows:

$$a_0 = a_0 - \frac{1}{2}\beta_0, b_0 = \beta_0 \tag{21}$$

$$a_n = \frac{1}{2}[(n+2)a_n - \delta_n], b_n = \frac{1}{2}[(n+2)\beta_n - \eta_n] \tag{22}$$

$$c_n = \frac{1}{2}(\delta_n - n a_n), d_n = \frac{1}{2}(\eta_n - n\beta_n) \tag{23}$$

In the actual calculation, the infinite series solution of (10) is not available, while the form of finite sum is available. In order to ensure that the final surface strictly meets the boundary conditions, the spectral approximation method is employed. In Eq. (10), r^n will decrease gradually with the increase of n until it can be ignored. Using the spectral approximation technique, Eq. (10) can be expressed as

$$u(r,\theta) = \frac{a_0}{2} + \frac{b_0}{4} r^2 + \sum_{n=1}^{M-1} r^n \left[\left(a_n + c_n r^2\right)\mathrm{cosn}\theta + \left(\mathrm{b_n} + \mathrm{d_n r^2}\right)\mathrm{sinn}\theta\right] + R(r,\theta) \tag{24}$$

where $R(r,\theta)$ is the remainder, representing the contribution of higher order terms to the solution. When M is large enough, $R(r,\theta)$ can be ignored inside the surface. In order for the surface to strictly meet the given boundary

conditions, this item must be retained, but some approximate form is available, such as

$$R(r,\theta) = A_1(\theta)r^M + A_2(\theta)r^{M+2} \tag{25}$$

where $A_1(\theta)$ and $A_2(\theta)$ are pending function. For simplicity, we denote:

$$F(r,\theta) = \frac{a_0}{2} + \frac{b_0}{4}r^2 + \sum_{n=1}^{M-1} r^n\left[\left(a_n + c_n r^2\right)\cos n\theta + \left(b_n + d_n r^2\right)\sin(n\theta)\right]$$

$$\Delta f(\theta) = f(\theta) - F(1,\theta)$$

$$\Delta g(\theta) = g(\theta) - F_r'(1,\theta) \tag{26}$$

In order to get the solution of the boundary value problem to satisfy the boundary conditions, $R(r,\theta)$ must satisfy the following conditions:

$$A_1(\theta) + A_2(\theta) = f(\theta) - F(1,\theta) = \Delta f(\theta) \tag{27}$$

$$MA_1(\theta) + (M+2)A_2(\theta) = \Delta g(\theta) \tag{28}$$

so we can obtain:

$$A_1(\theta) = \Delta f(\theta) - A_2(\theta) \tag{29}$$

$$A_2(\theta) = \frac{1}{2}[\Delta g(\theta) - M\Delta f(\theta)] \tag{30}$$

Based on the above derivation, we can develop an algorithm for constructing the Biharmonic-based surface, the algorithm is illustrated in Table 1.

As illustrated in Fig. 7, based on the proposed algorithm, the smooth surface G that is bounded by three generated Bezier curves B_0, B_1 and B_2 can be generated.

The above computational process can be iterated for each curve area CF_i in the curve network until a closed solid surface can be generated inside the provided polyhedron, as shown in Fig. 8a. The whole procedure is repeated for each polyhedron generated by the Voronoi tessellation to produce a packing of solid particles with smooth surfaces, as illustrated in Fig. 8b. Compared with the conventional random deposition method for particle packing, this method can generate more densely packed

Table 1 Algorithm for constructing the Biharmonic-based surface

Algorithm 1	
1	Compute the Fourier coefficient of the first M terms of $f(\theta)$ and $g(\theta)$ by fast Fourier transform
2	Compute $F(1,\theta)$ and $F_r'(1,\theta)$ by Eq. (26)
3	Compute $A_1(\theta)$ and $A_2(\theta)$ by Eqs. (29) and (30)
4	Compute coordinates of points on the surface by $u(r,\theta) = F(r,\theta) + R(r,\theta)$

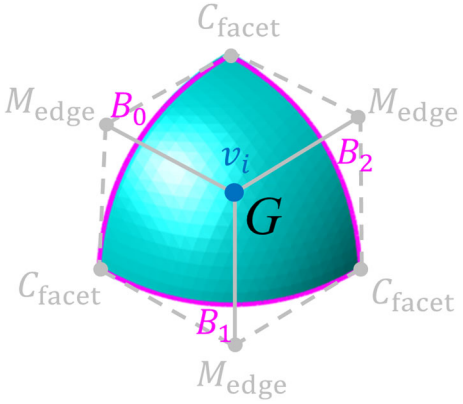

Fig. 7 The generated smooth surface bounded by three Bezier curves using the proposed biharmonic-equation-based method

particles, which are potentially contacted with their neighbors, whose Voronoi cells are in contact. The contact conditions between particles are influenced by the geometry of the generated Voronoi cells and the generated shapes of the particles. If two neighboring particles are smooth in surface (without addition of spherical harmonics noise), they will be contacted at the center of the facet that is shared by their Voronoi cells, and the contact condition (corner–corner contact, plane–corner contact) will be determined according to the local curvature of the two particle surface.

2.4 Producing concavity with spherical harmonics

Based on the above procedure, irregular convex granular particles with smooth surfaces are generated. Since the surface of a real particle frequently exhibits concavity features, the spherical harmonics are employed here to introduce extra concavity features onto the smooth surface of each generated particle.

The spherical harmonic transform (SHT), which is essentially a (2D) Fourier transform onto 3D sphere [5], has shown potential for characterizing the shapes of granular particles [16]. Previous researchers [38, 49, 54] have indicated that an inverse operation of SHT can be performed to reconstruct a virtual particle with specified shape features based on the presumed harmonic coefficient matrices. The idea of the SHT is to expand the polar radius of the particle surface from a unit sphere and to calculate the associated coefficients of the spherical harmonic series:

$$r(\theta,\varphi) = \sum_{n=0}^{N}\sum_{m=-n}^{n} c_n^m Y_n^m(\theta,\varphi) \tag{31}$$

where $r(\theta,\varphi)$ is the polar radius from the particle center with the corresponding spherical coordinates $\theta \in [0,\pi]$ and $\varphi \in [0,2\pi]$, which can be obtained by the coordinate

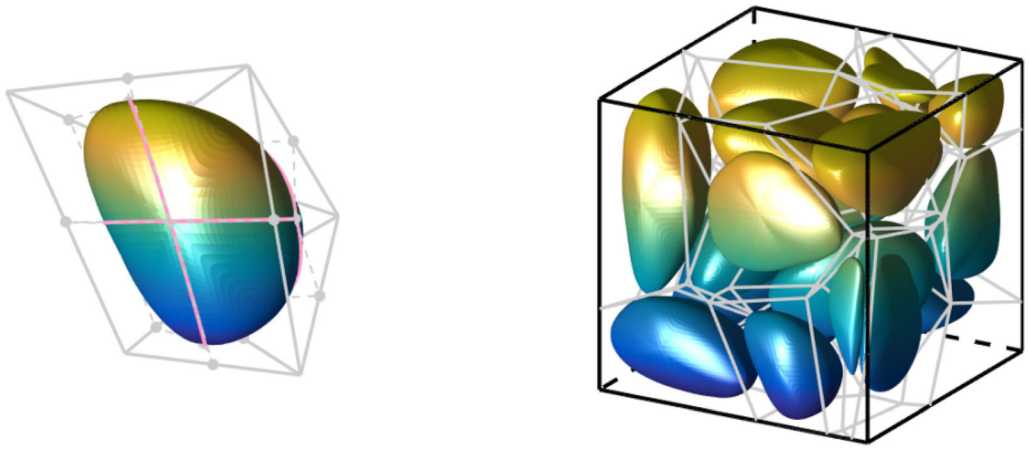

(a) **(b)**

Fig. 8 The generated solid particle with closed surface for **a** single particle case, and **b** multiple particles case

transformation of the particle surface vertices $V(x, y, z)$. c_n^m is the associated harmonic coefficient that requires determination, N is the total number of harmonic frequencies, and $Y_n^m(\theta, \varphi)$ is the spherical harmonic function given by:

$$Y_n^m(\theta, \varphi) = \sqrt{\frac{(2n+1)(n-m)!}{4\pi(n+m)!}} P_n^m(cos\theta) e^{im\varphi} \tag{32}$$

where n and m are the frequency and the order of the associated Legendre function $P_n^m(x)$, respectively, which can be expressed by Rodrigues's formula:

$$P_n^m(x) = \left(1-x^2\right)^{|m|/2} \cdot \frac{d^{|m|}}{dx^{|m|}} \left[\frac{1}{2^n n!} \cdot \frac{d^n}{dx^n}\left(x^2-1\right)^n\right] \tag{33}$$

According to Eq. (31), the total number of c_n^m is $(N+1)^2$. Taking the discrete values of $r(\theta, \varphi)$ as the input on the left side of Eq. (31), a linear equation system with $(N+1)^2$ unknowns is obtained. Then the optimized solution of c_n^m can be easily determined by adopting the standard least-squares estimation for the linear equation system. Finally, the inverse operation of SHT can be conducted to reconstruct the particle through the input of the obtained harmonic coefficients c_n^m on the right side of Eq. (31) to compute the reconstructed continuous surface points $r'(\theta, \varphi)$.

Previous works have shown that particle morphological features can be constructed by accumulating the decomposed spherical harmonic series with certain number of frequencies and specified amplitudes. According to [49], the amplitude of the input harmonic coefficients c_n^m at each frequency n determines different aspects of the reconstructed morphological features. The amplitude A_n at each frequency n can be computed as:

$$A_n = \sqrt{\sum_{m=-n}^{n} \|c_n^m\|^2} \tag{34}$$

where $\|c_n^m\|$ is the second-order norm of c_n^m.

Specifically, as stated in [49], A_0 represents the particle size, A_1 does not influence the spherical harmonic-reconstructed particle morphology, A_2 to A_4 represent the general shape of the particle at a large-scale level, and A_5 to A_{15} represent the local concavity feature at a small-scale level.

Based on the inverse operation of SHT as introduced above, the spherical harmonic series (when $5 \le n \le 15$) with coefficients c_n^m of amplitudes A_5 to A_{15} are employed to introduce concavity features to the generated smooth particle surface. According to [49], a linear relationship between A_n and n ($5 \le n \le 15$) in the log–log scale is assumed here:

$$A_n = K_A \cdot r_{ave} \cdot \left(\frac{n}{2}\right)^{2FD-6} \text{when}, 5 \le n \le 15 \tag{35}$$

where K_A is the parameter that controls the amplitudes of the harmonic coefficients at frequencies from 5 to 15, r_{ave} is the average radius of the generated smooth surface particle, and FD is the fractal dimension coefficient, which can be selected from the typical FD value ranges of Leighton Buzzard sand ($2.043 \le FD \le 2.169$) and highly decomposed granite ($2.195 \le FD \le 2.377$), as recommend by [49].

The procedure to produce concavity features on the generated convex particle is detailed as follows:

(1) Discretize the smooth surface of the generated convex shape particle into densely distributed discrete points. Transform the coordinates of the points from the Cartesian coordinate system into the spherical coordinate system;
(2) Calculate the mean radius of the surface points r_{ave};
(3) Determine the desired A_n $(5 \le n \le 15)$ based on Eq. (22) and the selected K_A and FD;
(4) Generate a series of random numbers for the normalized harmonic coefficients at each degree n, $c'_n = \left(c'^{-n}_n, c'^{-n+1}_n, \ldots, c'^{0}_n, \ldots, c'^{n-1}_n, c'^{n}_n\right)$ where c'^{m}_n $(-n \le m \le n)$ are random variables uniformly distributed from -1 to 1;
(5) Calculate the normalized amplitude of the random harmonic coefficients:

$$A'_n = \sqrt{\sum_{m=-n}^{n} \left(c'^{m}_n\right)^2} \tag{36}$$

(6) Determine the final harmonic coefficients c_n at each degree:

$$c_n = \left(c_n^{-n}, c_n^{-n+1}, \ldots, c_n^{0}, \ldots, c_n^{n-1}, c_n^{n}\right) \tag{37}$$

$$c_n^m = \frac{A_n}{A'_n} c'^{m}_n \tag{38}$$

(7) Calculate $Y_n^m(\theta, \varphi)$ for $\theta \in [0, \pi]$ and $\varphi \in [0, 2\pi]$ following Eq. (19), and calculate $r'(\theta, \varphi)$ based on $r(\theta, \varphi)$, c_n^m, $Y_n^m(\theta, \varphi)$, r_{ave} and the following equation:

$$r'(\theta, \varphi) = r(\theta, \varphi) \cdot \left[1 + \left(\sum_{n=5}^{15} \sum_{m=-n}^{n} c_n^m Y_n^m(\theta, \varphi) / r_{ave}\right)\right] \tag{39}$$

Figure 9 shows a unit sphere $r_{ave} = 1$ with imposed concavity features generated by the proposed spherical harmonic series at $n = 5$ to $n = 15$ for different K_A values.

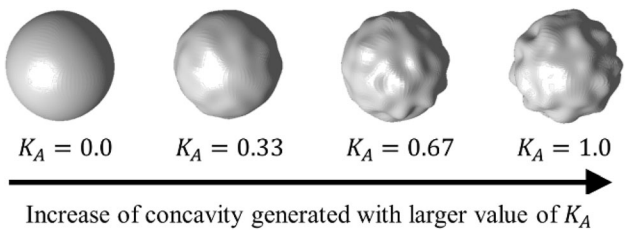

Fig. 9 Producing concavity on a sphere based on the proposed inverse operation of SHT with various K_A values

3 Control of the generated particle geometry

This section aims to illustrate how the volumetric size and different shape features of the generated particles can be quantitatively and independently controlled based on the relationship between the conventional geometry descriptors and the control parameters of the proposed algorithm.

3.1 Control of size and form parameters

First, we focus on the size and the form shape of the particle. The size of the particle, denoted as average radius, r_{ave}, is computed from the radius of an equivalent sphere with the same volume:

$$r_{ave} = \left(\frac{3V}{4\pi}\right)^{\frac{1}{3}} \tag{40}$$

For the form shape, the elongation index, (EI), and flatness index, (FI), are employed to quantify the dimensional ratio of the particle:

$$EI = \frac{I}{L} \tag{41}$$

$$FI = \frac{S}{I} \tag{42}$$

where S, I, and L are the minor, intermediate and major principal dimension of the particle, respectively.

Since the generated particle approximates the given polyhedron to some extent, r_{ave}^{gen} EI^{gen} and FI^{gen} are expected to be correlated with those of the circumscribed polyhedron, r_{ave}^{poly}, EI^{poly} and FI^{poly}, respectively. Figure 10a-c illustrates some example particles, which are generated inside polyhedrons of various r_{ave}^{poly}, EI^{poly} and FI^{poly} values. It can be seen from the figure that the polyhedrons with higher r_{ave}^{poly}, EI^{poly} and FI^{poly} values tend to produce particles with higher r_{ave}^{gen} EI^{gen} and FI^{gen} values, respectively.

To further verify the capability to adjust the sizes and form shapes by controlling of the polyhedron geometry, 1000 polyhedrons of various sizes $(r_{ave}^{poly} \in [1, 5])$, elongations $EI_{ave}^{poly} \in [0.2, 1]$ and flatness values $FI_{ave}^{poly} \in [0.2, 1]$ are generated. For each polyhedron, a random variable w that follows a uniform distribution ranging from 0.1 to 1.0 is assigned to generate the smooth surface particle. Then, the r_{ave}^{gen}, EI^{gen}, FI^{gen} values for all the particles are computed. The influences of (a) r_{ave}^{poly}, (b) EI^{poly} and (c) FI^{poly} on the obtained r_{ave}^{gen}, EI^{gen}, and FI^{gen}, respectively, are shown in Fig. 11. As expected, r_{ave}^{poly}, EI^{poly} and FI^{poly} exhibit a strong linear relation with r_{ave}^{gen}, EI^{gen}, and FI^{gen}, respectively. The equations of the generated size and shape

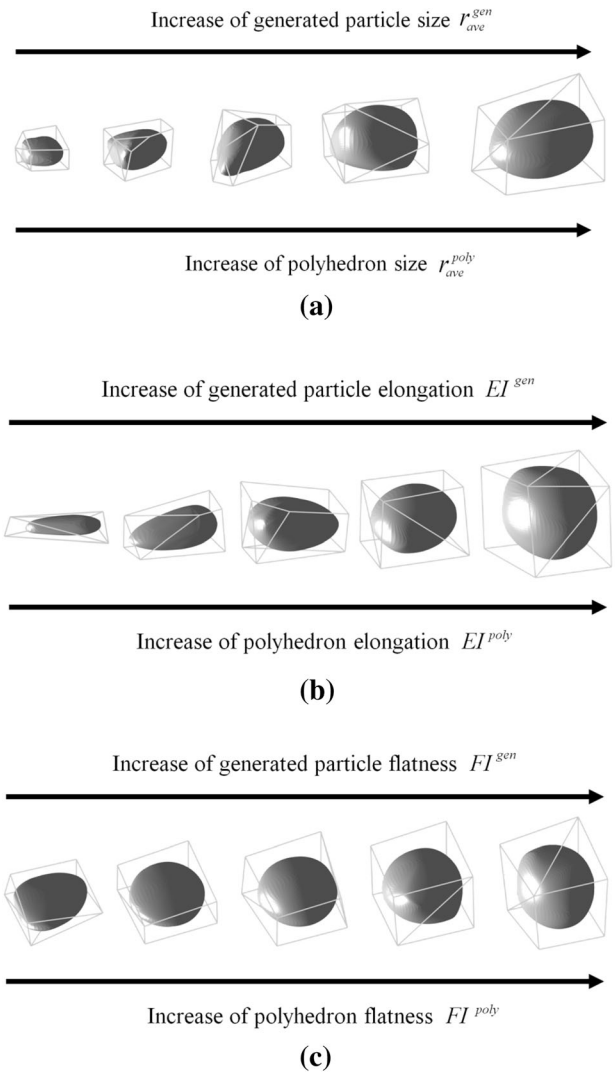

Fig. 10 Illustration of example particles generated inside polyhedron of various **a** r_{ave}^{poly}, **b** EI^{poly} and **c** FI^{poly}

values of particles as the functions of the corresponding control parameters of polyhedrons are obtained from regression analysis and are listed as follows:

$$r_{ave}^{gen} = 0.770 r_{ave}^{poly} - 0.037 \tag{43}$$

$$EI^{gen} = 0.872 EI^{poly} + 0.852 \tag{44}$$

$$FI^{gen} = 0.853 FI^{poly} + 0.989 \tag{45}$$

Based on the above equations, r_{ave}^{poly}, EI^{poly} and FI^{poly} can thus be used to control the preliminary size and form shapes of the generated particle. More accurate control can be implemented based on the inverse adjustment of individual polyhedron geometry as detailed in the author's previous work [26] and concluded in Sect. 4.1.

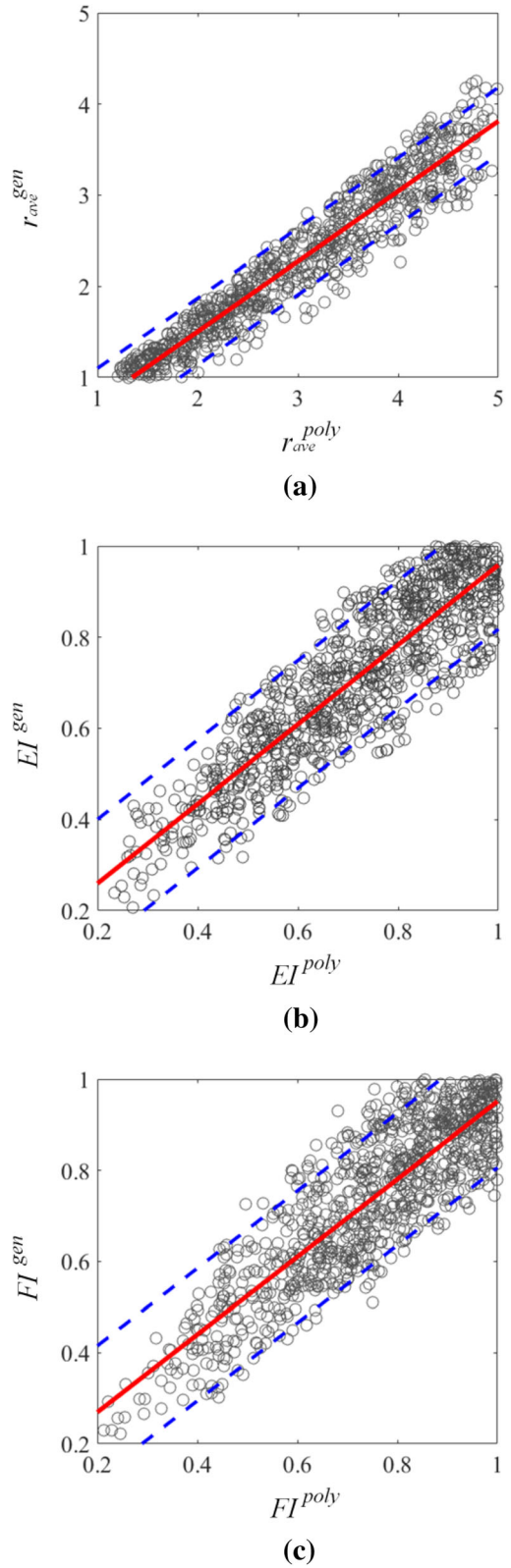

Fig. 11 Influences of control parameters **a** r_{ave}^{poly}, **b** EI^{poly} and **c** FI^{poly} on the **a** r_{ave}^{gen}, **b** EI^{gen} and **c** FI^{gen} of the generated particles. Solid line: mean values; dotted lines: mean values +/- one standard deviation

3.2 Control of the corner sharpness parameter

The sharpness of the corners is known to influence the kinematics, e.g., sliding and rolling [45], of the particles. In this section, we illustrate the capability of the proposed algorithm to control the corner sharpness of the generated particle. The 3D Wadell's roundness is computed to quantify the corner sharpness [30]:

$$R = \frac{\sum r_i}{nR_{insc}} \tag{46}$$

where R_{insc} is the radius of the maximum inscribed circle, r_i is the radius of the ith sphere which is fitted to the corner of the particle, and n is the total number of spheres that fit all the identified particle corners. Figure 12 illustrates four example particles with various corner sharpness values generated by different value of w, where w ranges from 0.1 to 0.4, and R increases from 0.16 to 0.65.

To further verify the capability of adjusting the corner sharpness with the control parameter w, 1000 polyhedrons of various elongation and flatness are generated. For each polyhedron, a random variable w that follows a uniform distribution ranging from 0.1 to 1.0 is assigned to generate the smooth surface particle of different corner sharpness features. Then, the R values for all the particles are computed. The influences of w on the obtained R values, as well as those on EI^{gen} and FI^{gen}, are shown in Fig. 13. As expected, R exhibits a strong inverse-U-shape relation with w. Based on the obtained data, the polynomial regression equation for relating w to R is derived as follows:

$$R = -1.563w^3 + 0.038w^2 + 1.698w - 0.063 \tag{47}$$

Thus, with the above equation and inverse parameter adjustment, w can be used to control the corner sharpness R of the generated particle.

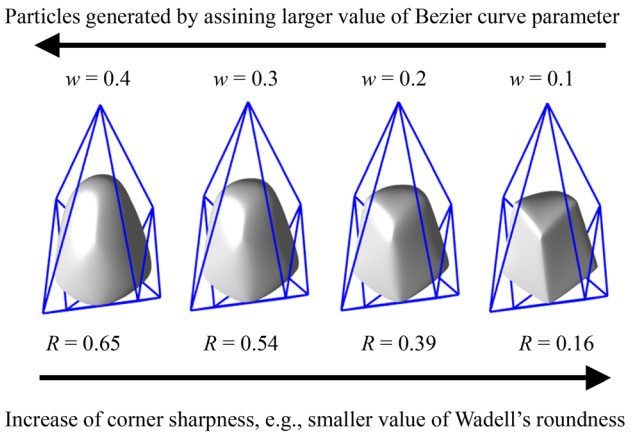

Fig. 12 Example particle of various corner sharpness generated by different value of w

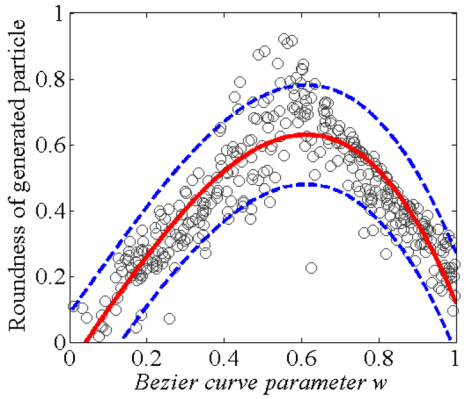

Fig. 13 Influence of control parameter w on roundness of generated particles. Solid line: mean values; dotted lines: mean values +/- one standard deviation

3.3 Control of concavity parameter

The convexity ratio (CR) characterizes the concavity feature, which is known to influence the amount of interlocking at contacts between two neighboring particles. For a 3D particle, it is calculated as:

$$CR = \frac{V_{particle}}{V_{convex}} \tag{48}$$

where $V_{particle}$ is the volume of the particle and V_{convex} is the volume of the convex hull of the particle. In this section, we illustrate the capability of the proposed algorithm to reproduce particles with desired concavity features using the spherical harmonics of different control parametersK_A. First, the example particles generated by different control parameters w and K_A are shown in Fig. 14.

To further verify the capability of adjusting the particle concavity, the correlations between the convexity ratio of the generated particles and the control parameter K_A are examined. In this section, the previously generated 1000

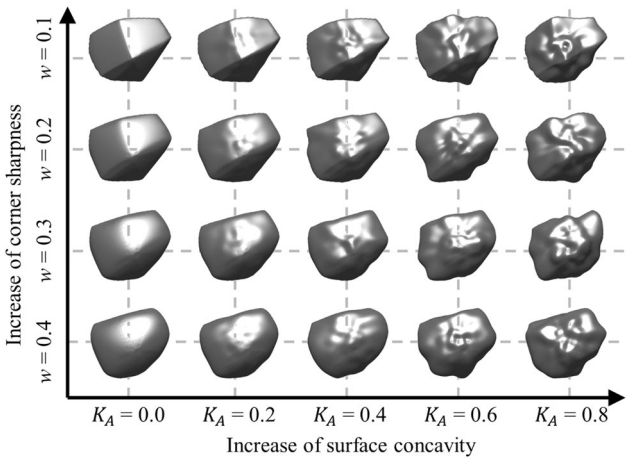

Fig. 14 Illustration of particles generated by different control parameters w and K_A

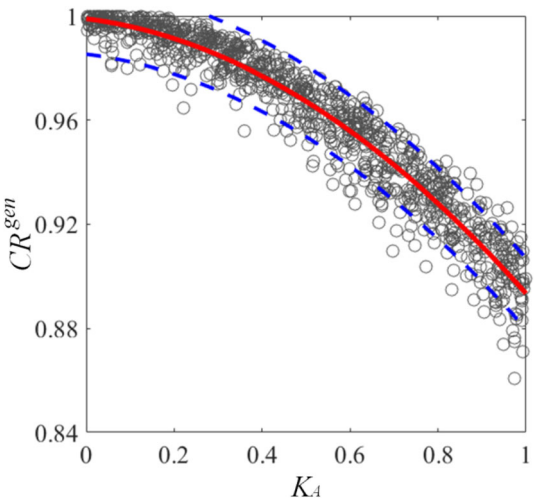

Fig. 15 Influence of control parameter K_A on concavity of generated particles (CR^{gen}). Solid line: mean values; dotted lines: mean values +/- one standard deviation

smooth surface particles ($CR = 0$) with various elongation, flatness and roundness values are used as the parent particles. For each parent, 10 particles are generated with various values of K_A, which follows a uniform distribution ranging from 0 to 1.0. The influences of K_A on the obtained CR^{gen} are shown in Fig. 15. As expected, the K_A exhibits a strong negative relation with CR^{gen}. The regression equation for controlling of CR^{gen} with K_A can be obtained:

$$CR^{gen} = -0.026{K_A}^3 - 0.493{K_A}^2 - 0.146K_A - 0.999 \quad (49)$$

Subsequently, using this equation, when the desired convexity ratio CR^{tar} is given, the corresponding K_A can be easily determined. If there is any discrepancy between the generated convexity ratio CR^{gen} and the target value, the inverse adjustment can always be performed to accurately control the error.

4 Random packing of the generated irregular particles

4.1 Proposed scheme for generation of particle packing

In this study, the proposed algorithm to generate the random packing of non-spherical particles with desired geometric features includes the following major steps:

(i) First, irregular-shaped polyhedrons with desired size, elongation and flatness values are generated through the constrained Voronoi tessellation method [26]. The method is alternative to the normal Voronoi tessellation method and is based on the controlled partition of the virtual container by the means of a constrained Voronoi tessellation. The method was inspired by the IMC framework that initially appeared in [18]. The constrained Voronoi tessellation comprises the following sub-steps:

  (i) Generate an initial set of points within the selected domain, and perform a bounded Voronoi tessellation (i.e., the union of all the cells is identical to the whole domain).
  (ii) Evaluate the geometric properties of the obtained Voronoi polyhedron, e.g., $r_{\text{ave}}^{\text{poly}}$, EI^{poly} and FI^{poly}. Compute the error corresponding to the differences between the current values and the targets, ($r_{\text{ave}}^{\text{tar}}$, EI^{tar} and FI^{tar}).
  (iii) Randomly move one of the seeding points to another random location, compute the new tessellation with only modifying the local cells around the moving point [26], and repeat step (ii). If the error is less than its previous value, accept the modification; otherwise, reject it.
  (iv) Repeat step (iii) until the error has reached an acceptable value. Indeed, there would still be a certain discrepancy between the generated particles and the targets. Thus, the above procedure can be performed again to minimize the error between those the generated particles ($r_{\text{ave}}^{\text{gen}}$, EI^{gen} and FI^{gen}), and the desired targets, ($r_{\text{ave}}^{\text{tar}}$, EI^{tar} and FI^{tar}).

(2) Next, the key points are extracted from the edges and facets of the polyhedrons. According to the target corner sharpness (R^{tar}), the Bézier curves are generated with certain control parameter w to form curve networks inside the polyhedrons. Then, an irregular non-spherical particle surface is generated based on biharmonic surface interpolation.

(3) Based on the target convexity (CR^{tar}), superimpose the spherical harmonics with appropriate K_A values on the particle surface to produce convexity features.

(4) Finally, compute the error corresponding to the differences between the current and target ones. Adjust the shape control parameters w, and K_{A}, until the error reaches an acceptable value.

4.2 Examples of generated particle packing

To comprehensively demonstrate the capability of the proposed algorithms for studying granular materials, three scenarios of particle packing are provided in this subsection: (1) packing of bidispersed particle mixtures with

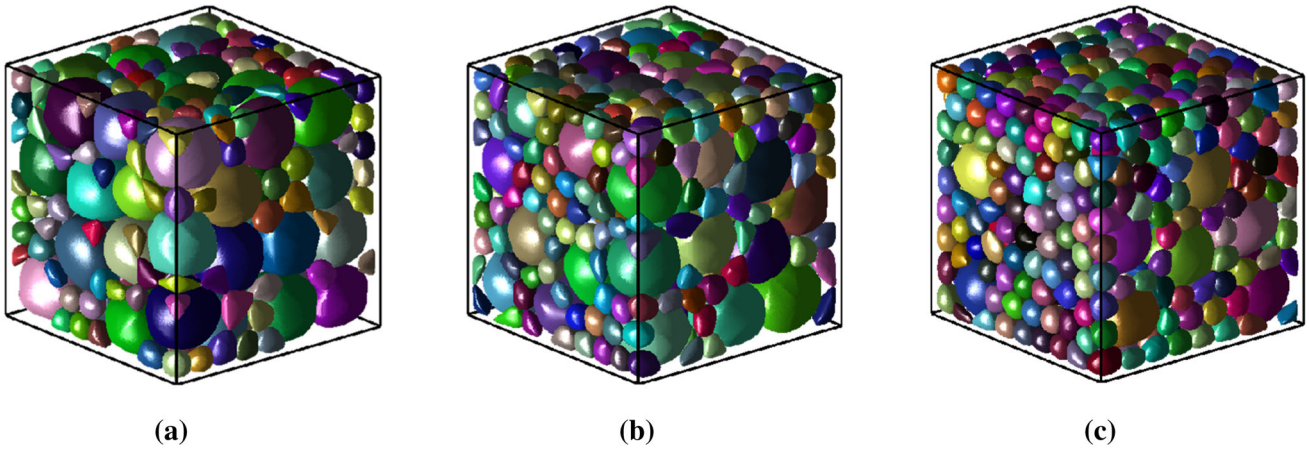

Fig. 16 Packing patterns of the generated binary mixture with different volumetric size ratio **a** $W_C = 80\%$, **b** $W_C = 60\%$ and **c** $W_C = 40\%$

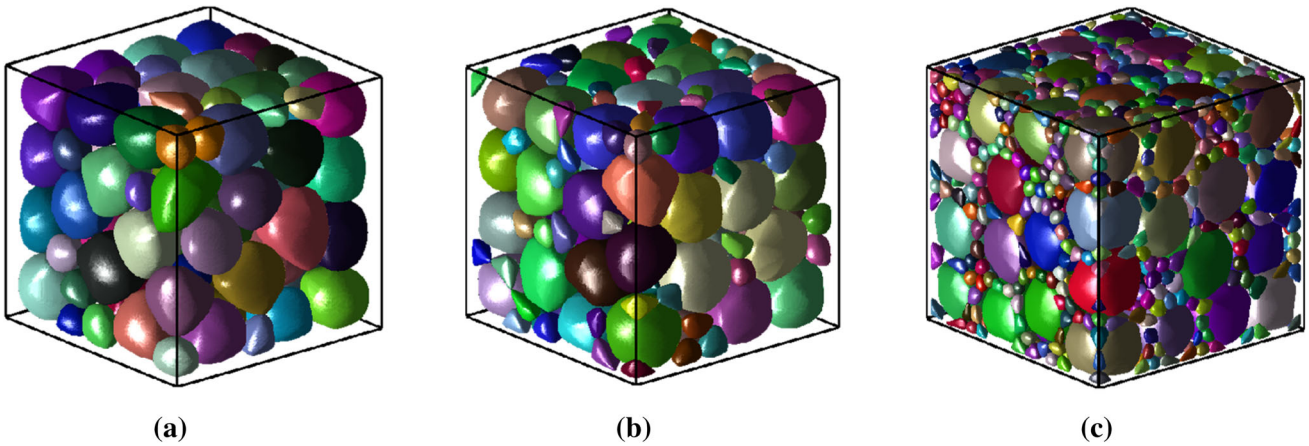

Fig. 17 Packing patterns of the generated binary mixture with different volumetric size ratio **a** $\alpha_V = 5:3$, **b** $\alpha_V = 5:2$ and **c** $\alpha_V = 5:1$

various coarse-particle weights and different size ratios, (2) packing of realistic particles with distinctive shape features, and (3) packing of quantitatively controlled particle orientations and form-scale shapes.

(1) Packing of bidispersed particle mixtures.

Bidispersed particle mixtures with various combinations of coarse and fine grains are simulated using the proposed method. The simulated particles can be considered as binary mixtures of sands and gravels with sufficiently large interparticle stiffness and cohesionless interparticle contacts. The binary mixture can be characterized by two important parameters: the weight of the coarse grains, W_C, and the grain size ratio, α_V:

$$W_C = \frac{V_{coarse}}{V_{total}} \tag{50}$$

where V_{coarse} represents the sum of the volume of the coarse particles and V_{total} represents the total volume of the coarse and fine particles, and

$$\alpha_V = \frac{\mu(D_{coarse})}{\mu(D_{fine})} \tag{51}$$

where $\mu(D_{coarse})$ denotes the mean diameter of the coarse grains and $\mu(D_{fine})$ denotes the mean diameter of the fine grains.

In total, 6 samples are produced to illustrate the capability of the proposed method to simulate bidispersed particles with different values of W_C and α_V. The bidispersed binary particle mixtures have different coarse grain weights ($W_C = 80\%$, 60%, 40%) and grain size ratios ($\alpha_V = 1:1, 2:1, 3:1$); the packing patterns are illustrated in Fig. 16 and Fig. 17, respectively. The figures show that the proposed method can efficiently and effectively produce bidispersed particle mixtures with various coarse grain weights and grain size ratios. Since many geotechnical researchers are very interested in binary mixture (gap graded soils) and the generation of initial packing for such material was the main problem that influences the computational time in their simulations, we demonstrate the bi-

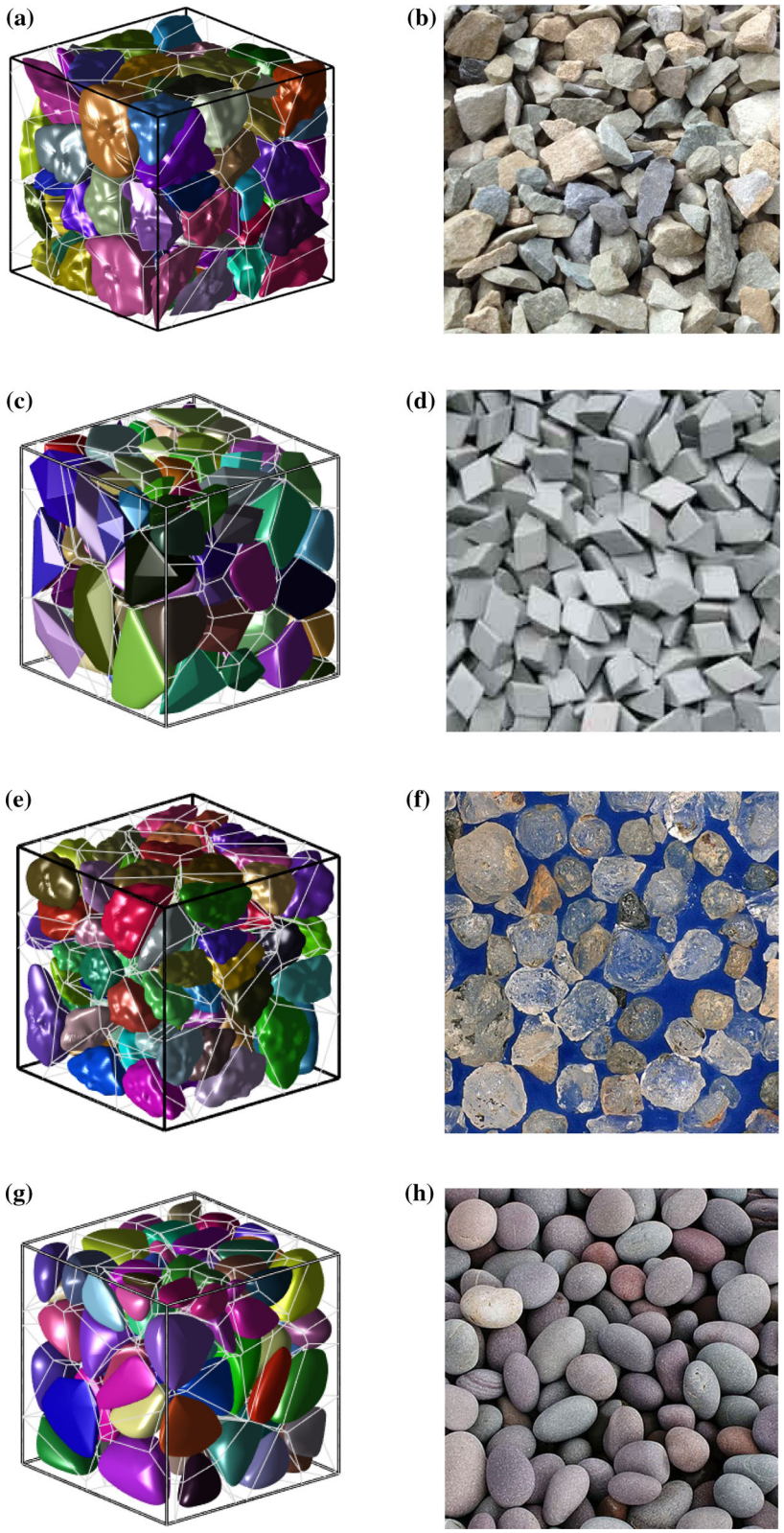

Fig. 18 Four examples of packing with distinctive particle shapes

disperse packings for illustration purpose. It should be noted that the algorithm can actually generate a wide range of particle size distribution. The capability and validity of

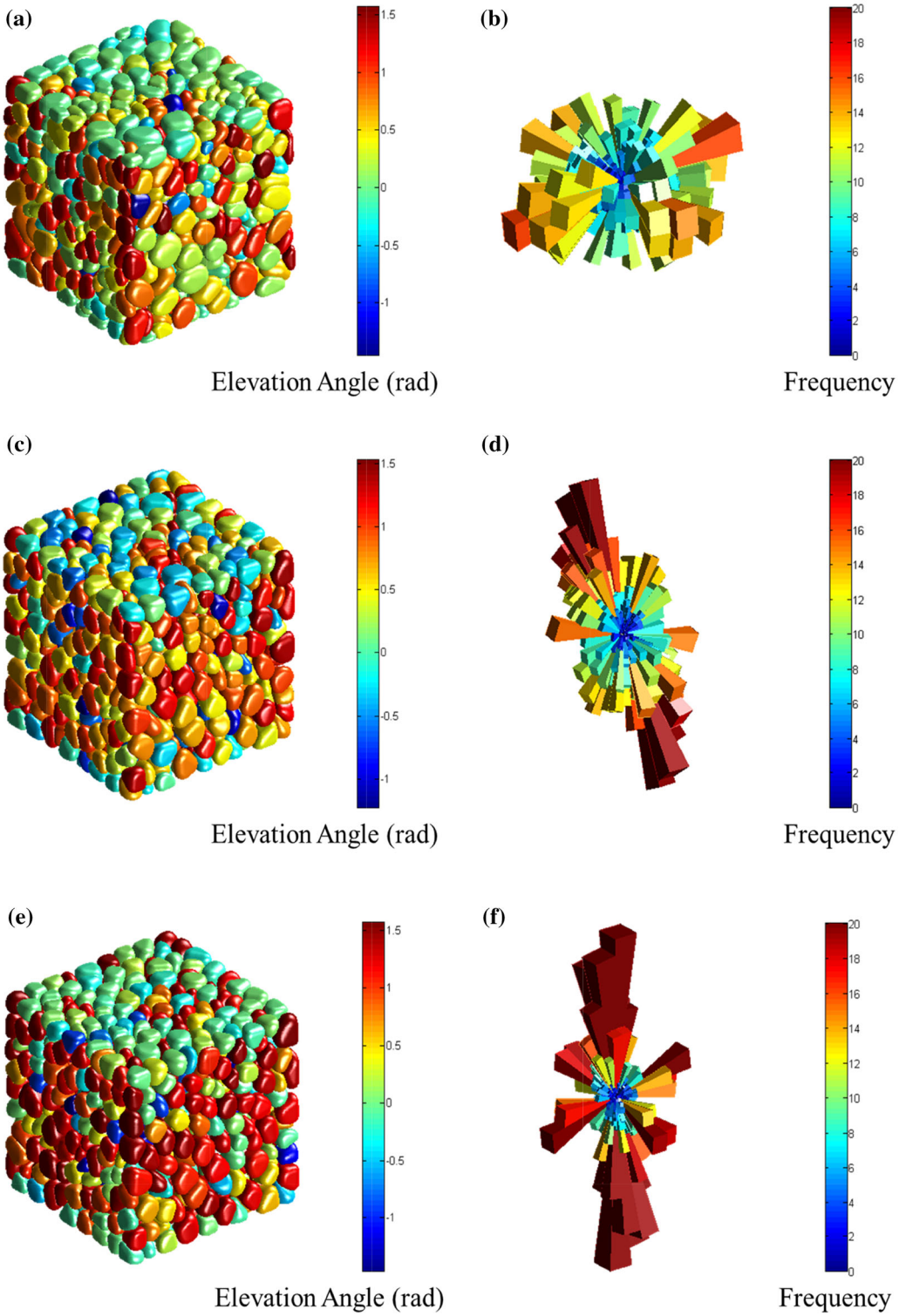

Fig. 19 Generation of vertical orientated particles: **a**, **b** initial stage; **c**, **d** intermediate stage; **e**, **f** final stage

the IMC algorithm to control the Voronoi cell size distributions are detailed in [26].

(2) Packing of particles that have realistic shapes.

Four examples of particle packing, composed of 100 particles each, are generated with the following realistic and distinctive features: (1) the first example aims to generate particles with high corner sharpness and large

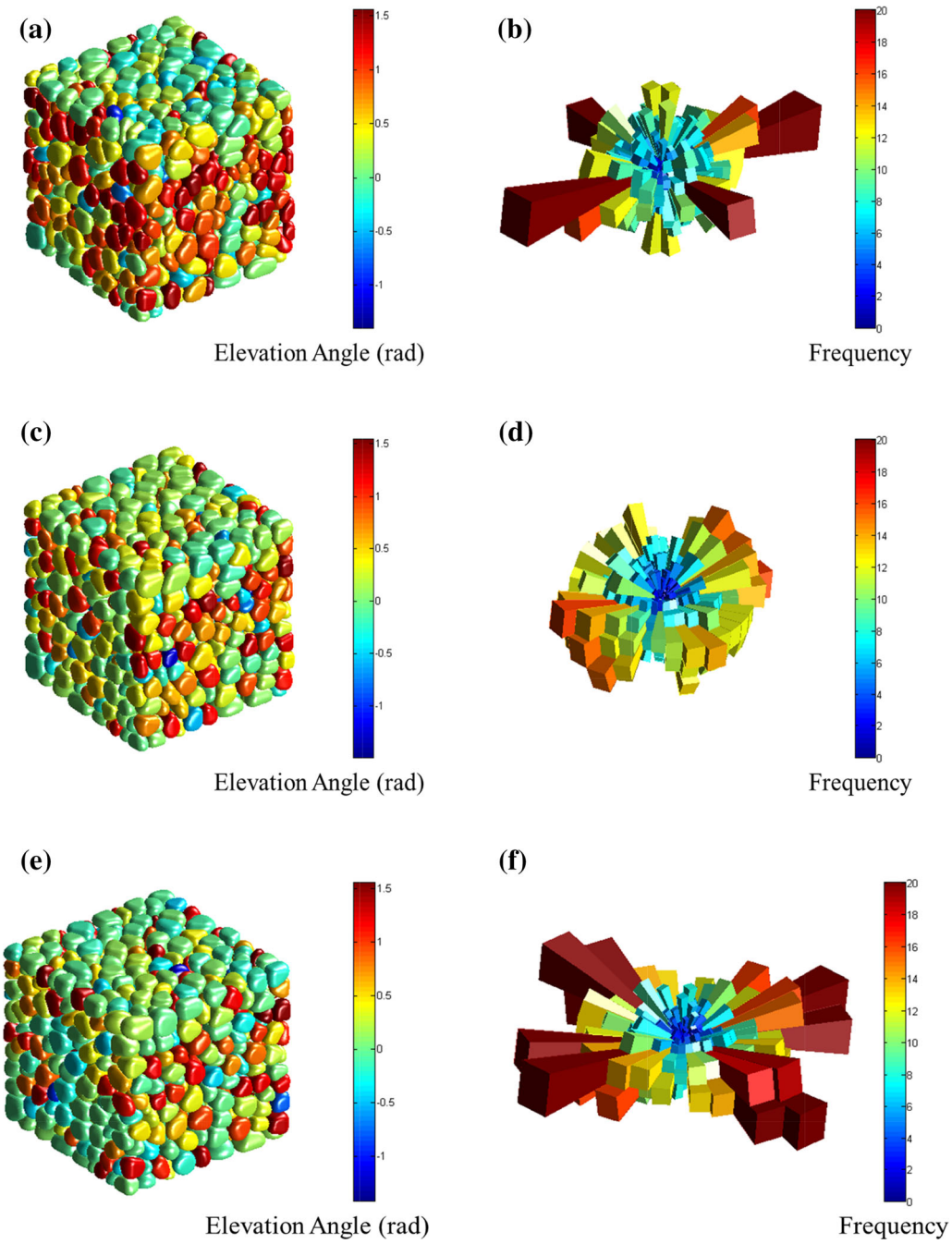

Fig. 20 Generation of horizontal orientated particles: **a**, **b** initial stage; **c**, **d** intermediate stage; **e**, **f** final stage

concavity values, (2) the second example focuses on producing particles with sharp corners without concavity, (3) the third example generates particles with low corner sharpness with larger concavity, and (4) the fourth example produces particles with rounded corners and smooth surfaces. The properties related to the corner sharpness and concavity are acquired by carefully adjusting the control parameters w and K_A. The clearly recognizable differences between the four examples are visualized in Fig. 18a-h. The grain shapes of the first example are somehow similar to those of crushed rocks in Fig. 18b, while those of the second example are more often encountered in grinding materials, e.g., the brown fused alumina in Fig. 18d. The shapes of the third example approximate those of the quartz sands, in Fig. 18f, while the particles in the fourth example are more identical to riverbank pebbles, in Fig. 18h.

(3) Packing of particles having prescribed geometrical values.

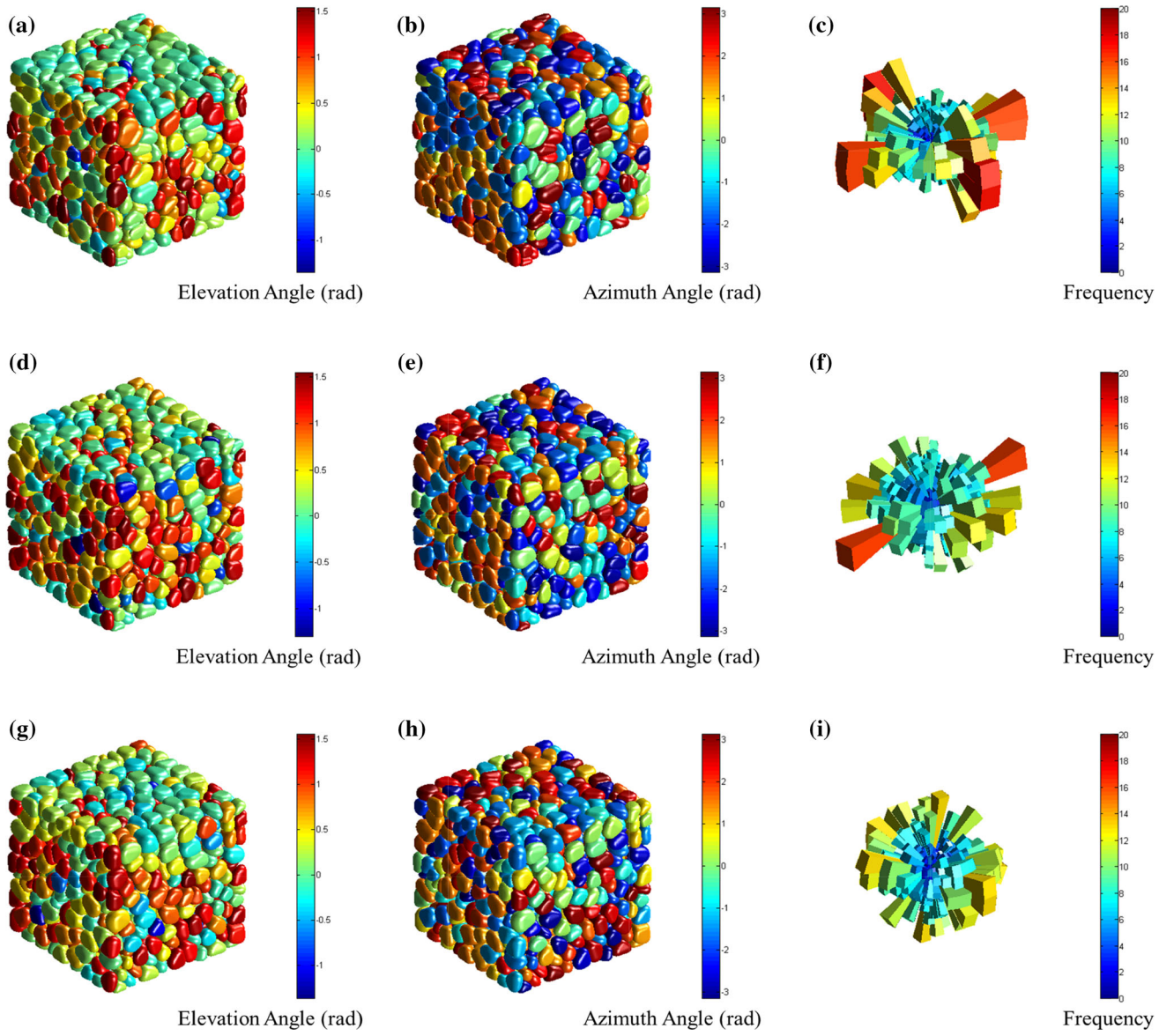

Fig. 21 Generation of isotropic orientated particles: **a**, **b** initial stage; **d–f** intermediate stage; **g–i** final stage

Two groups of particle packing are presented at this scenario to illustrate the potential of proposed algorithm. They make use of the illustrative geometry controlling scheme as presented in the previous sections. Each group has the following prescribed distinctive features:

Group 1: Particles with desired orientations, e.g., isotropic orientated ($\theta \in [-\pi, \pi]$, $\varphi \in \left[-\frac{\pi}{2}, \frac{\pi}{2}\right]$), vertical orientated ($\theta \in [-\pi, \pi]$, $\varphi \to -\frac{\pi}{2}$ or $\frac{\pi}{2}$), and horizontal orientated ($\theta \in [-\pi, \pi]$, $\varphi \to 0$).

As illustrated in Fig. 19a-b, at initial stage, the reconstructed particles based on the Voronoi cells tend to have random orientations. Then, after a few numbers of iterations, as shown in Fig. 19c-d, the generated particles gradually become vertically orientated. The final results are demonstrated in Fig. 19e-f, where the particles assembly displays identical orientations to the desired values, $\theta \in [-\pi, \pi]$, $\varphi \to -\frac{\pi}{2}$ or $\frac{\pi}{2}$.

The evolutions of the generated particles and their orientation diagrams for horizontal orientated and isotropic orientated spatial distributions are illustrated in Fig. 20 and Fig. 21, respectively. The results prove that the proposed algorithm has good performance in generating particles packing with predetermined spatial orientations.

Group 2: Particles with desired elongations and flatness, e.g., oblate ($\mu_{EI} = 0.9$, $\sigma_{EI} = 0.06$; $\mu_{FI} = 0.5$, $\sigma_{FI} = 0.06$), prolate ($\mu_{EI} = 0.5$, $\sigma_{EI} = 0.06$; $\mu_{FI} = 0.9$, $\sigma_{FI} = 0.06$) and scalene ($\mu_{EI} = 0.5$, $\sigma_{EI} = 0.06$; $\mu_{FI} = 0.5$, $\sigma_{FI} = 0.06$). The error function between the generated *EI*, *FI* distributions and their corresponding targets are defined as:

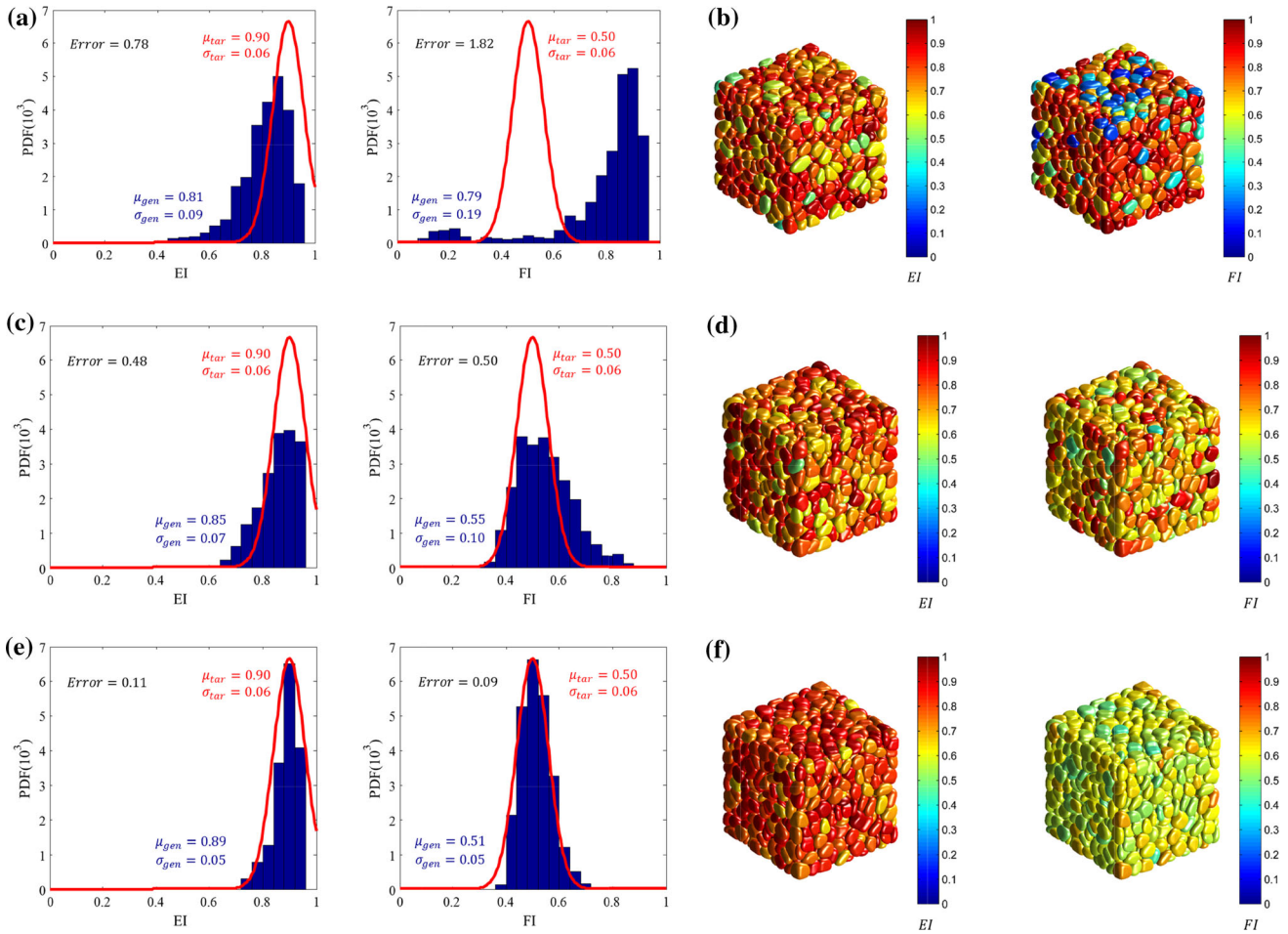

Fig. 22 Generation of oblate shape particles:: **a**, **b** initial stage; **c**, **d** intermediate stage; **e**, **f** final stage

$$\text{Error} = \int_0^1 \left| pdf_{tar}(x) - pdf_{gen}(x) \right| dx \tag{52}$$

where $pdf_{tar}(x)$ is the target probability density function of the chosen shape index and $pdf_{gen}(x)$ is the generated probability density function of the chosen shape index. Following the author's previous work in [27], the integral is computed numerically using discretized versions of the probability density function, and a target value of 0.1 can provide satisfactory results.

As displayed in Fig. 22a-b, at the initial stage, the particles reconstructed from the original Voronoi cells exhibit quite random distributions of elongation and flatness, $EI \in [0.4, 1.0]$, $FI \in [0.1, 1.0]$. The errors between the generated EI, FI values and their corresponding targets were 0.78 and 1.82, respectively. Then, after the geometry adjustment algorithm is applied, as illustrated in Fig. 22c-d, the mean value of elongation increases from 0.81 to 0.85, while the mean of flatness significantly decreases from 0.79 to 0.55. The errors for both EI and FI also decrease to about 0.5. Finally, as illustrated in Fig. 22e-f, the generated specimen exhibits EI and FI values approach very close to the desired distributions, with satisfied errors around 0.1.

As for the prolate and scalene cases, the changes of the shape distributions from initial stage to final stage, which are processed by the proposed algorithm, are also illustrated in Fig. 23 and Fig. 24, respectively. The generated prolate particles present errors of EI and FI decreasing from 1.83 to 0.11 and 0.54 to 0.14, while the generated scalene particles exhibit errors of EI and FI reducing from 1.84 to 0.11 and 1.83 to 0.09. They both display statistics of generated particle shapes gradually become identical to the predetermined distributions. The above examples prove that the proposed algorithm has very strong capability in generating particles packing that satisfies the prescribed targets of particle shapes.

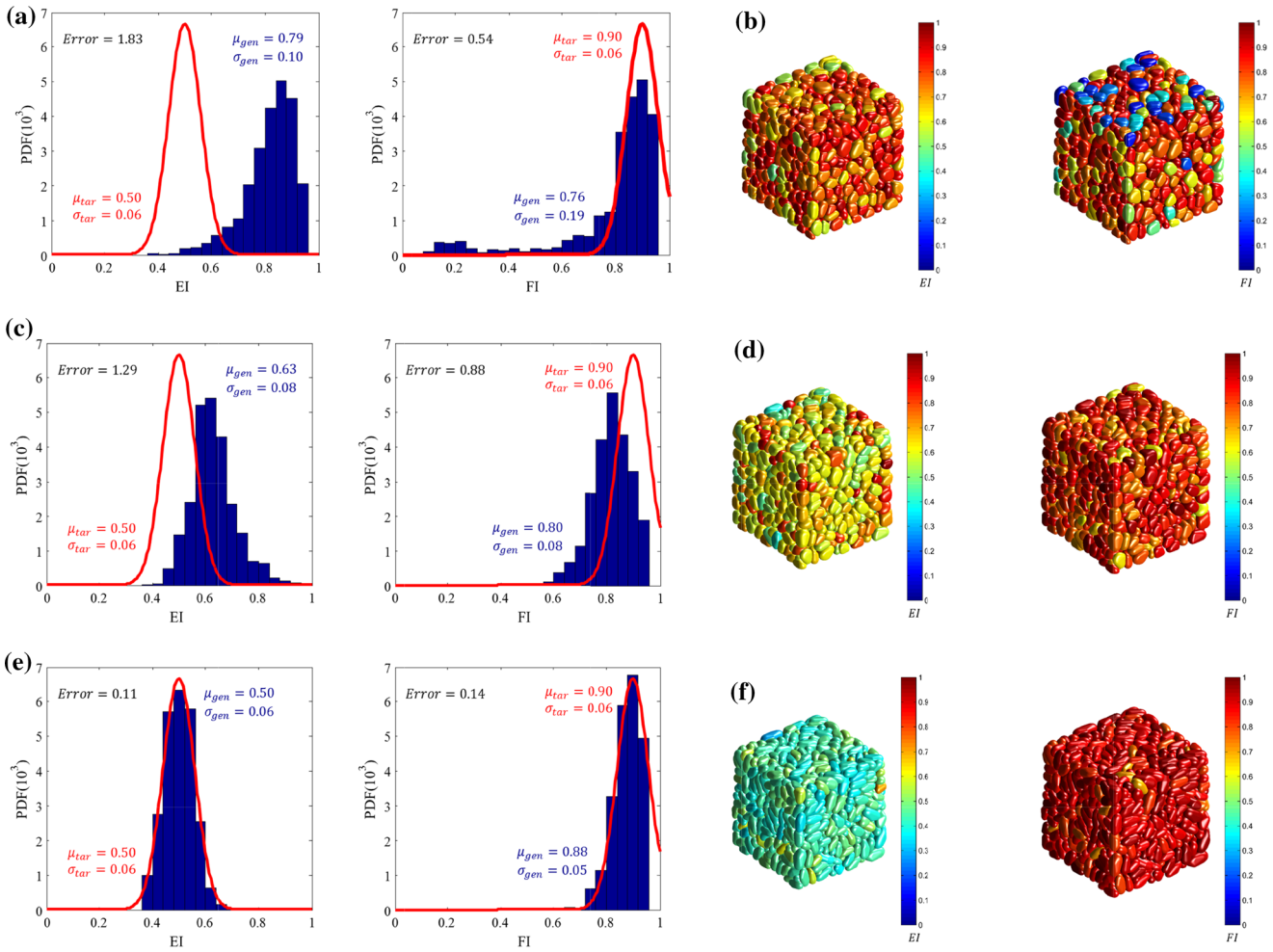

Fig. 23 Generation of prolate shape particles: **a**, **b** initial stage; **c**, **d** intermediate stage; **e**, **f** final stage

5 Conclusion and discussion

In this paper, we proposed and combined a series of computational geometry algorithms (Voronoi tessellation, Bezier curve fitting and biharmonic-based surface interpolation) and spherical harmonic transformation for generation of non-spherical particles with controllable shape features for future numerical investigation of shape effects on granular behaviors. The quantitative control of size, elongation, flatness, corner sharpness and concavity is facilitated through the geometry modification of Voronoi polyhedron and adjustment of the control parameters w and K_A for particle generation. Three cases of particles packing are given to demonstrate the capabilities of the proposed approach. The first case illustrates the ability of proposed approach in producing bidispersed particle mixtures with various coarse grain weights and grain size ratios. The second case shows the capability of generating packing of realistic particles with distinctive shape features. The third case validates the geometry controlling capability of the prosed algorithms. All results prove that the proposed method is robust and efficient in generating realistic granular packing with desired grain sizes and distinctive particle shapes. It provides a basis for numerical simulation of different shape effects of natural granular materials on their mechanical, thermal and hydraulic properties.

In conclusion, the sample generation is a very important step of discrete element modeling, in particular for irregular particles and initial anisotropy of the sample. This study only focuses on the sample generation relating to the geometrical aspect of granular packing, and the part of granular mechanics will be followed in a future study. Indeed, there is a major challenge in implementation of further numerical tests on the generated packing of particles in DEM. How to simulate irregular particles with concave and convex shapes effectively and efficiently is still an open problem. Potential solutions include overlapping-spheres-based DEM [12], NURBS-based DEM [3], level-set-based DEM [21], etc. However, the computational loads of these discrete modeling techniques increase

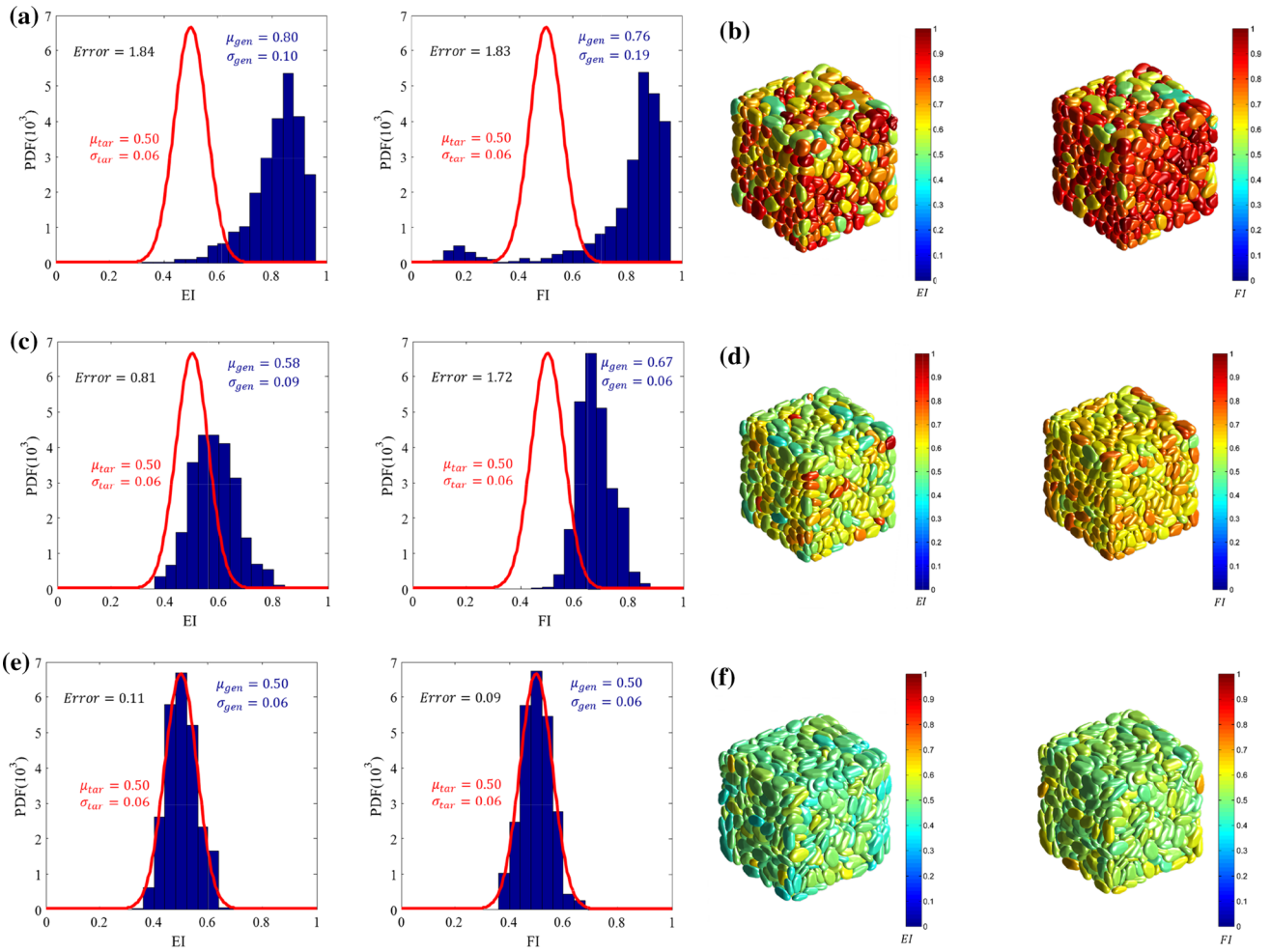

Fig. 24 Generation of scalene shape particles: **a**, **b** initial stage; **c**, **d** intermediate stage; **e**, **f** final stage

markedly with the increasing complexity of the particle outline. Additionally, there will be a trade-off between the number of spheres/nodes and the fidelity of the simplified particle profile compared with the original one. The simplifications should not alter the shape properties of interests. Based on the present work, our future research will focus on: (1) incorporation of the proposed particle model into DEM code, e.g., developing an advancing contact detection approach that is suitable for arbitrary shape particles; (2) investigating the individual effects of shapes, e.g., corner sharpness and concavity on the macro- and micromechanical properties of granular materials based on the proposed particle models.

Acknowledgments This research was supported by the National Natural Science Foundation of China (Nos. 51878416, 51938008, 52090081). RGC HONG KONG (Grant No.:15209119, R5037-18F). The authors would like to express their appreciation to these sources of financial assistance.

Compliance with ethical standards

Conflict of interest We declare that we have no financial and personal relationships with other people or organizations that can inappropriately influence our work, and there is no professional or other personal interest of any nature or kind in any product, service and/or company that could be construed as influencing the position presented in, or the review of, the manuscript entitled "A novel approach of random packing generation of complex-shaped 3D particles with controllable sizes and shapes".

References

1. Altuhafi FN, Coop MR (2011) Changes to particle characteristics associated with the compression of sands. Geotechnique 61:459–471
2. Altuhafi FN, Coop MR, Georgiannou VN (2016) Effect of Particle Shape on the Mechanical Behavior of Natural Sands. J Geotech Geoenviron Eng 142(12):04016071

3. Andrade JE, Lim K-W, Avila CF, Vlahinić I (2012) Granular element method for computational particle mechanics. Comput Methods Appl Mech Eng 241–244:262–274
4. Azéma E, Radjaï F (2010) Stress-strain behavior and geometrical properties of packings of elongated particles. Phys Rev E: Stat Nonlin Soft Matter Phys 81:051304
5. Blais JR, Soofi MA (2006) Spherical harmonic transforms using quadratures and least squares. In: International Conference on Computational Science. Springer, Berlin, Heidelberg, pp 48–55
6. Boon C, Houlsby G, Utili S (2013) A new contact detection algorithm for three-dimensional non-spherical particles. Powder Technol 248:94–102
7. Chaikittisilp W, Taenumtrakul T, Boonsuwan P, Tanthapanichakoon W, Charinpanitkul T (2006) Analysis of solid particle mixing in inclined fluidized beds using DEM simulation. Chem Eng J 122:21–29
8. Coetzee CJ (2016) Calibration of the discrete element method and the effect of particle shape. Powder Technol 297:50–70
9. Cundall PA, Strack OD (1979) A discrete numerical model for granular assemblies. Geotechnique 29(1):47–65
10. Dong K, Wang C, Yu A (2015) A novel method based on orientation discretization for discrete element modeling of non-spherical particles. Chem Eng Sci 126:500–516
11. Eliáš J (2014) Simulation of railway ballast using crushable polyhedral particles. Powder Technol 264:458–465
12. Ferellec JF, Mcdowell GR (2010) A method to model realistic particle shape and inertia in DEM. Granular Matter 12:459–467
13. Fortune S (1987) A sweepline algorithm for Voronoi diagrams. Algorithmica 2:153–174
14. Fu XW, Huck D, Makein L, Armstrong B, Willen U, Freeman T (2012) Effect of particle shape and size on flow properties of lactose powders. Particuology 10:203–208
15. Gan JQ, Yu AB, Zhou ZY (2016) DEM simulation on the packing of fine ellipsoids. Chem Eng Sci 156:64–76
16. Garboczi EJ (2002) Three-dimensional mathematical analysis of particle shape using X-ray tomography and spherical harmonics: application to aggregates used in concrete. Cement Concrete Research 32:1621–1638
17. Gong J, Liu J (2017) Mechanical transitional behavior of binary mixtures via DEM: effect of differences in contact-type friction coefficients. Comput Geotech 85:1–14
18. Gross D, Li M (2002) Constructing microstructures of poly- and nanocrystalline materials for numerical modeling and simulation. Appl Phys Lett 80:746–748
19. Han K, Feng YT, Owen DRJ (2006) Polygon-based contact resolution for superquadrics. Int J Numer Methods Eng 66(3):485–501
20. He Y, Evans TJ, Yu A, Yang R (2018) A GPU-based DEM for modelling large scale powder compaction with wide size distributions. Powder Technol 333:219–228
21. Kawamoto R, Andò E, Viggiani G, Andrade JE (2016) Level set discrete element method for three-dimensional computations with triaxial case study. Comput Methods Appl Mech Eng 91:1–13
22. Kyrylyuk AV, Philipse AP (2011) Effect of particle shape on the random packing density of amorphous solids. Phys Status Solidi 208:2299–2302
23. Li J, Webb C, Pandiella SS, Campbell GM (2003) Discrete particle motion on sieves—a numerical study using the DEM simulation. Powder Technol 133:190–202
24. Lin X, Ng TT (1995) Contact detection algorithms for three-dimensional ellipsoids in discrete element modelling. Int J Numer Anal Meth Geomech 19:653–659
25. Lin X, Ng TT (1997) A three-dimensional discrete element model using arrays of ellipsoids. Géotechnique 47:319–329
26. Mollon G, Zhao J (2012) Fourier–Voronoi-based generation of realistic samples for discrete modelling of granular materials. Granular Matter 14:621–638
27. Mollon G, Zhao J (2014) 3D generation of realistic granular samples based on random fields theory and Fourier shape descriptors. Comput Methods Appl Mech Eng 279:46–65
28. Nassauer B, Liedke T, Kuna M (2013) Polyhedral particles for the discrete element method. Granular Matter 15:85–93
29. Ng T-T (1994) Numerical simulations of granular soil using elliptical particles. Comput Geotech 16:153–169
30. Nie Z, Liang Z, Wang X (2018) A three-dimensional particle roundness evaluation method. Granular Matter 20:32
31. Oda M, Konishi J, Nemat-Nasser S (1982) Experimental micromechanical evaluation of strength of granular materials: Effects of particle rolling. Mech Mater 1:269–283
32. Peng L, Li SX, Jian Z, Meng LY (2010) A computational investigation on random packings of sphere-spherocylinder mixtures. Sci China Phys Mech Astron 53:2284–2292
33. Peters JF, Hopkins MA, Kala R, Wahl RE (2009) A poly-ellipsoid particle for non-spherical discrete element method. Eng Comput 26:645–657
34. Recarey C, Pérez I, Roselló R, Muniz M, Hernández E, Giraldo R, Oñate E (2019) Advances in particle packing algorithms for generating the medium in the Discrete Element Method. Comput Methods Appl Mech Eng 345:336–362
35. Rothenburg L, Bathurst RJ (1992) Micromechanical features of granular assemblies with planar elliptical particles. Geotechnique 42(1):79–95
36. Santamarina JC, Cho GC (2004) Soil behaviour: the role of particle shape. In: Advances in geotechnical engineering: the skempton conference. Thomas Telford Publishing, pp 604–617
37. Sitharam TG, Nimbkar MS (2000) Micromechanical modelling of granular materials: effect of particle size and gradation. Geotech Geol Eng 18:91–117
38. Su D, Yan WM (2020) Prediction of 3D size and shape descriptors of irregular granular particles from projected 2D images. Acta Geotech 15:1533–1555
39. Su D, Yan WM (2017) 3D characterization of general-shape sand particles using microfocus X-ray computed tomography and spherical harmonic functions, and particle regeneration using multivariate random vector. Powder Technol 323:8–23
40. Tong L, Wang YH (2015) DEM simulations of shear modulus and damping ratio of sand with emphasis on the effects of particle number, particle shape, and aging. Acta Geotech 10:117–130
41. Tsomokos A, Georgiannou VN (2010) Effect of grain shape and angularity on the undrained response of fine sands. Can Geotech J 47:539–551
42. Tsuji Y, Kawaguchi T, Tanaka T (1993) Discrete particle simulation of two-dimensional fluidized bed. Powder Technol 77:79–87
43. Tutumluer E, Huang H, Hashash YM, Ghaboussi J (2008) Imaging based discrete element modeling of granular assemblies. Am Inst Phys 973(1):544–549
44. Ueda T, Matsushima T, Yamada Y (2011) Effect of particle size ratio and volume fraction on shear strength of binary granular mixture. Granular Matter 13:731–742
45. Vangla P, Roy N, Gali ML (2018) Image based shape characterization of granular materials and its effect on kinematics of particle motion. Granular Matter 20(1):1–19
46. Vepraskas MJ, Cassel DK (1987) Sphericity and roundness of sand in coastal plain soils and relationships with soil physical properties. Soil Sci Soc of Am J 51(5):1108–1112
47. Wang X, Gong J, An A, Zhang K, Nie Z (2019) Random generation of convex granule packing based on weighted Voronoi tessellation and cubic-polynomial-curve fitting. Comput Geotech 113:103088

48. Wang L, Li R, Wu B, Wu Z, Ding Z (2018) Determination of the coefficient of rolling friction of an irregularly shaped maize particle group using physical experiment and simulations. Particuology 38:185–195
49. Wei D, Wang J, Nie J, Zhou B (2018) Generation of realistic sand particles with fractal nature using an improved spherical harmonic analysis. Comput Geotech 104:1–12
50. Yang Y, Wang JF, Cheng YM (2016) Quantified evaluation of particle shape effects from micro-to-macro scales for non-convex grains. Particuology 25:23–35
51. Zhao S, Zhang N, Zhou X, Zhang L (2017) Particle shape effects on fabric of granular random packing. Powder Technol 310:175–186
52. Zhou B, Wang J, Zhao B (2015) Micromorphology characterization and reconstruction of sand particles using micro X-ray tomography and spherical harmonics. Eng Geol 184:126–137
53. Zhou W, Huang Y, Ng TT, Ma G (2018) A geometric potential-based contact detection algorithm for egg-shaped particles in discrete element modeling. Powder Technol 327:152–162
54. Zhou B, Wang J (2017) Generation of a realistic 3D sand assembly using X-ray micro-computed tomography and spherical harmonic-based principal component analysis. Int J Numer Anal Meth Geomech 41(1):93–109
55. Zhu H, Zhou Z, Yang R, Yu A (2008) Discrete particle simulation of particulate systems: a review of major applications and findings. Chem Eng Sci 63(23):5728–5770